EFFICACY OF HEATED HYDROUS ETHANOL INJECTION FOR IMPROVING
EMISSIONS FROM DUAL FUEL DIESEL ENGINES

A THESIS
SUBMITTED TO THE FACULTY OF
UNIVERSITY OF MINNESOTA
BY

Alex Nord

IN PARTIAL FULFILLMENT OF THE REQUIREMENTS
FOR THE DEGREE OF
MASTER OF SCIENCE

Advised By: Professor William F. Northrop

May 2017

Acknowledgements

Dedication

I would like to dedicate this thesis to Steve Ullrich, the most influential teacher I have had throughout my education. Steve taught the Engineering I, II, and III classes at Lakeville South High School. He was also the head of Lakeville South's FIRST robotics team. The engineering classes he taught provided students with the opportunity to work with Pro/ENGINEER, a 3D modeling and product development software. Between these engineering classes and the robotics team, there was a dominant factor of using this modeling software. As a result, for myself and other students like me, our creativity was fueled and thus paved the way for the birth of our engineering mindsets. It is because of Mr. Ullrich's influence on me that I was driven to become an engineer and strived to further my education through graduate school. Although I was one of his many students, he has without a doubt changed my world. For that I will forever be grateful.

Abstract

With emissions standards becoming ever more stringent, aftermarket dual-fuel solutions are being developed to allow legacy diesel engines to reach higher regulatory emissions tiers. Manufacturers are reluctant to adopt dual-fuel systems due to perceived lack of consumer interest. However, the use of aftermarket dual-fuel systems with partially renewable fuels has sparked interest in limited markets. Previous research has shown slight emissions reduction benefits from fumigation with 120 proof hydrous ethanol in a diesel engine using a commercially available dual-fuel system. However, the findings do not match manufacturer claims of emissions reductions. The work presented here examines the design, development, performance, and emissions from an engine equipped with a novel aftermarket port fuel injection (PFI) dual fuel system with a fuel heating system integrated into the fuel injector rail. Finite element modeling techniques in ANSYS were used to optimize the heat exchanger and analyze its performance. In addition, cross-sections and flow path lines were created in ANSYS to examine thermal profiles and flow turbulence at varying ethanol flow rates. A John Deere 4045HF475 Tier 2 diesel engine was retrofitted with a custom PFI rail designed to inject hydrous ethanol with the ability to preheat the ethanol using circulated hot engine coolant to improve the vaporization and mixing of the secondary fuel and air in the intake port. Port-injected fuel flow was controlled by varying injector pulse width and throttle position was adjusted manually to maintain testing mode parameters. Heated ethanol, unheated ethanol, and diesel only operating modes were run over a modified ISO 8178 eight-point test plan. Fumigant energy fraction (FEF), defined as the amount of energy provided by the fumigant based on the lower heating value (LHV)

divided by the total fuel energy, up to 37% was achieved in the experiments. Ethanol fuel rail heat exchanger effectiveness decreased with increasing FEF and log-mean temperature difference (LMTD) increased. These opposite effects were likely due to dimensional design constraints of the heat exchanger limiting the heat transfer. Experiments found that with increasing FEF, engine NO emissions decreased, whereas NO_2, CO, THC, and ethanol emissions increased. NO emissions reductions were countered by increasing NO_2, resulting in constant NO_X emissions. Soot concentrations produced varying trends, but with a tendency to decrease overall at high FEF. Preheating the ethanol with circulated engine coolant yielded few benefits to engine out-emissions. This study showed that the dual-fuel heated PFI rail system provided modest emissions benefits over diesel-only operation. Preheating the liquid ethanol was not as successful as anticipated because ethanol's high latent heat of vaporization dominated over the sensible heat required to heat the liquid prior to the injectors.

Table of Contents

List of Tables

List of Figures

Nomenclature

A/F Ratio...Air/Fuel Ratio

ATDCF ....After Top Dead Center Firing

BMEP..Brake Mean Effective Pressure

BSFC...Brake Specific Fuel Consumption

BTE...Brake Thermal Efficiency

CAD ....Crank Angle Degree

CE ....Combustion Efficiency

CI...Compression Ignition

DDGS..Dried Distillers Grains and Solubles

DI ....Direct Injection

ε..Effectiveness

EGR...Exhaust Gas Recirculation

EVC...Exhaust Valve Close

EVO ....Exhaust Valve Open

FEF..Fumigant Energy Fraction

FT-IR...Fourier Transform Infrared Spectrometer

GDI ....Gasoline Direct Injection

GHG...Greenhouse Gas

HC ....Hydrocarbons

HCCI...Homogeneous-Charge Compression Ignition

IVC...Intake Valve Close

IVO ....Intake Valve Open

LFE ....Laminar Flow Element

LHV ....Lower Heating Value

LMTD ....Log-Mean Temperature Difference

MSS...Micro-Soot Sensor

NI ....National Instruments

PFI..Port Fuel Injection

PM..Particulate Matter

RCCI...Reactivity Controlled Compression Ignition

SCR..Selective Catalytic Reduction

SI..Spark Ignition

TEMA ....Tubular Exchanger Manufacturers Association

TDC..Top Dead Center

THC..Total Hydrocarbons

ULSD ....Ultra-Low Sulfur Diesel

Chapter 1: Introduction

1.1 Motivation

Vehicle emissions and fuel economy regulations are becoming ever more stringent requiring corresponding advancements in engine technology. Diesel engines have excellent longevity; therefore, engines over a decade old are likely to continue operating while newer equipment is introduced. Advanced combustion technologies such as single fuel homogeneous-charge compression ignition (HCCI) and premixed low temperature combustion (LTC), and dual fuel strategies like reactivity controlled compression ignition (RCCI) and fumigation have been explored for lowering engine out emissions while retaining engine efficiency and performance. Some techniques have shown promise for decreasing emissions while increasing efficiency but lead to practical disadvantages. For example, fumigation and PFI strategies dual fuel strategies can be installed as aftermarket options for diesel engines, whereas RCCI requires full control of engine parameters and must be implemented by an original equipment manufacturer (OEM).

Aftertreatment is the most common method for reducing emissions from diesel engines. Since diesel engines operate lean of stoichiometric, they cannot utilize three-way catalysts like gasoline engines and must use a series of catalytic reactors and filters. Oxidation catalysts are used for eliminating CO and HC emissions, selective catalytic reduction (SCR) is used to reduce NO_X emissions, and soot is trapped using particulate filters. Work has been conducted to allow the continued operation of legacy engines using aftermarket aftertreatment catalysts but available kits are costly and don't integrate well with exiting engine control systems. Aftermarket dual fuel systems offer an alternative

approach for reducing emissions from legacy engines while integrating more seamlessly with existing engine control systems.

U.S. No. 2 diesel prices have significantly increased over the last 16 years, peaking in July 2008 with a monthly average of $4.70/gal and averaging at $3.89/gal from 2011-2014 [1]. During this time, alternatives have been explored as blending components or substitutes for diesel fuel. Ethanol was identified as a promising choice due to its high octane number, which aids knock prevention and for its potential to decrease harmful emissions when combusted in engines [2]. In addition, ethanol is widely available biofuel in the US as it is a byproduct from corn stock production, and ethanol requires less input energy compared to diesel. Figure 1 shows the monthly report of diesel and ethanol fuel prices per gallon [1,3]. From 2000-2016, ethanol was 23% cheaper than diesel fuel on average, making it an attractive secondary fuel for dual fuel combustion strategies. Maximum fuel cost savings of up to 0.143% per percent of fumigant energy fraction (FEF), defined as the amount of energy provided by the fumigant based on the lower heating value (LHV) divided by the total fuel energy, was possible by replacing diesel with ethanol.
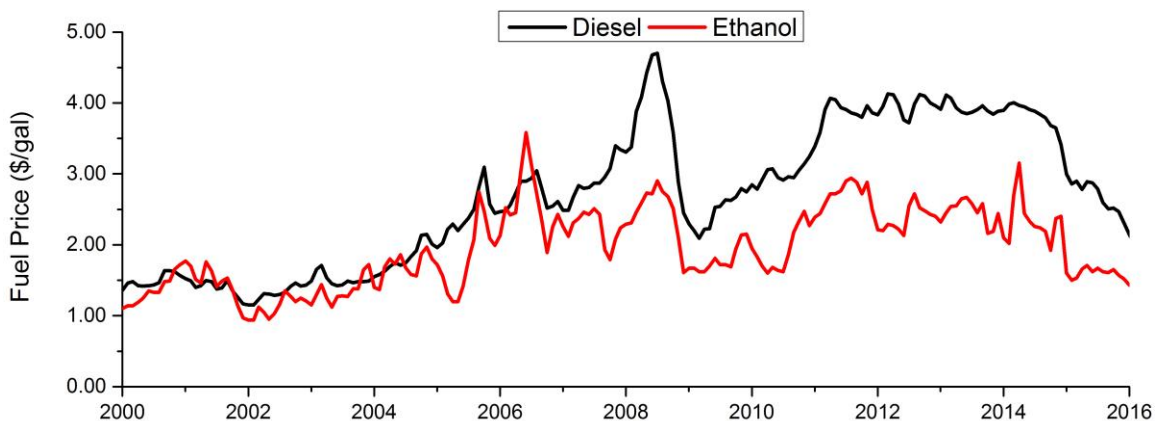
Figure 1: Diesel and ethanol fuel prices per gallon from 2000 to 2016 [1,3]

Previous research has been conducted incorporating an aftermarket dual fuel ethanol system which utilizes fumigation of 120 proof hydrous ethanol [4]. Hwang et al. found that high water content hydrous ethanol produces lower in cylinder temperatures. They hypothesized that higher ethanol concentrations may return better less variable combustion while retaining the emissions benefits from low combustion temperature. Lower ethanol proofs require less net energy to produce as compared to anhydrous ethanol. Saffy et al. found that in ethanol by removing the molecular sieve, 180 proof ethanol can be produced with upwards of 10% net energy saved through the stripping column and removal of the dehydration stage [5]. Ethanol is well known for its high latent heat of vaporization, which leads to a charge cooling effect and ignition delay.

This work investigates an aftermarket duel fuel system to allow use of higher ethanol proof and greater replacement of diesel fuel energy for a given engine load. Additional motivations for this system are to use PFI for its ability to be minimally invasive with the stock diesel equipment and to increase the injection temperature of the ethanol using circulated engine coolant to aid vaporization. It is hypothesized that combustion efficiency and emissions can be improved through these improvements.

1.2 Statement of Problem

Dual fuel diesel combustion strategies can benefit from the utilization of hydrous ethanol as the secondary fuel. Ethanol's high latent heat of vaporization reduces in-cylinder temperatures, which reduce NO_X emissions and increase knock resistance through charge cooling effect and high octane number. In addition, ethanol is a viable substitute for displacing diesel combustion. Working with a legacy diesel engine, it is more desirable to

3

use a less invasive approach such as fumigation. However, fumigation research has shown very low diesel replacement percentages, necessitating alternative means of injecting ethanol.

PFI is a viable option for increasing ethanol injection while not requiring significant engine modifications. In addition, PFI can control secondary fuel injection parameters more closely and the potential for better mixing of fuel and air. Little research has been done using PFI with ethanol as the secondary fuel. In turn, a system is to be produced that can analyze the results from PFI of low water content hydrous ethanol. A heat exchanger will need to be incorporated internally to preheat the ethanol for analysis of vaporization and mixing. The overall goals are to increase the achievable FEF range as compared to previous research studies, improve engine out emissions, and explore the benefits of preheating the ethanol prior to injection.

1.3 Significance

The objective of the work presented in this thesis was to design, fabricate, and analyze the performance of a novel heated PFI hydrous ethanol injection system. This system preheats the ethanol prior to injection by circulating hot engine coolant through a fuel rail with an integrated heat exchanger. The work aims to provide a better understanding of the effect of heated and unheated 180 proof hydrous ethanol on diesel engines using PFI strategies.

1.4 Organization

The organization of this thesis is as follows. A background review of dual fuel engine combustion and fuels, current diesel emissions standards, hydrous ethanol

production, and combustion research is presented. Next, the design process of the heat exchanger is detailed by analyzing the stock intake manifold, the optimization of the shell and tube configuration, and evaluating the final model through combinations of SolidWorks and ANSYS modeling. Then, the experimental apparatus is detailed, including engine and dynamometer specifications. Finally, the heat exchanger performance, engine performance, and engine out emissions are presented and discussed.

Chapter 2: Background

2.1 Combustion Alternatives and Fuel Fundamentals

Internal combustion engines are commonly categorized as either spark ignition (SI) or compression ignition (CI). Over the years, various combustion methods between these bounds have been tested with purported improvements in emissions or engine performance. Figure 2 shows a range of combustion methods, fuel, from primarily gasoline to primarily diesel.
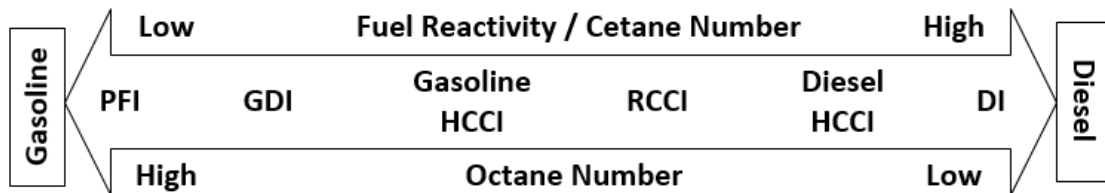
Figure 2: Fuel reactivity, cetane number, and octane number trends for various combustion methods [6]

According to Figure 2, gasoline and diesel fuels are on each end of the fuel reactivity spectrum; gasoline has a low reactivity, whereas diesel has a high reactivity. Cetane and octane numbers are common measures of fuel reactivity. Cetane number is an indicator of a fuel's ability to auto-ignite, whereas octane number is an indicator of a fuel's resistance to knocking and compression ignition. Cetane number and octane number have an inverse relationship and are independent of fuel composition [7]. PFI, gasoline direct injection (GDI), and gasoline HCCI can be achieved with gasoline and gasoline-like fuels. Likewise, diesel fuel is used in DI, diesel HCCI, or RCCI applications. Standard SI engines operate in a small range around stoichiometric combustion, whereas CI engines favor lean

6

combustion. For SI engines, the mixture of fuel and air will ignite most efficiently when well mixed prior to entering the cylinder head. Running fuel-rich can produce more power, and running fuel-lean can return better fuel economy. In CI engines, fuel is injected near the end of the compression stroke where it combusts almost instantly before being able to mix with air. If fuel is burned without enough oxygen, soot is formed at high temperatures. Adding more fuel produces more power but increases soot as well. To prevent soot formation, CI engines tend to operate with lean combustion to ensure enough air is supplied to the fuel being injected.

PFI is a widely-used strategy where fuel injectors are placed in the intake port and aimed at the back side of the valves. This strategy typically injects prior to the intake valve opening and takes advantage of the hot valve and surrounding port area to help vaporize the fuel. This vaporization aids mixing with intake air and combustion. A common concern of PFI is excess fuel short-circuiting to the exhaust due to valve overlap. This can lead to poor fuel economy and increased hydrocarbon (HC) emissions. McGee et al. examined the effects of aiming injectors and injection timing. They found that combustion is more stable when injectors are aimed directly at the valve and the intake valve is closed during injection. This increased fuel preparation and decreased the hydrocarbon emissions [8]. PFI strategies are often concerned with hydrocarbon emissions, however they commonly produce lower PM emissions when compared to GDI or conventional diesel engines [9,10].

GDI engines were in production during the late 1990's but became more prominent in the U.S. during 2008-2012 [11–13]. Compared to PFI, GDI has better control over fuel by placing the injector in the cylinder and using stratified injections. This results in a more

homogeneous mixture and overall better fuel economy. Other reasons for the rising popularity of GDI over PFI in SI engines can be attributed to the better vaporization of the fuel, causing a charge cooling effect. This often leads to increases in volumetric efficiency, engine power output, and overall engine efficiency, through the utilization of increased knock limits [14]. Ethanol's higher heat of vaporization causes a similar charge cooling effect for combustion. This cooling effect, coupled with its high octane number and molecular structure, gives ethanol a very high resistance to knock, making it a desirable secondary fuel for both DI, PFI, and fuel blends, for both SI and CI applications [15]. In dual fuel CI applications with ethanol, a diesel pilot injection is necessary to initiate the combustion of ethanol because it is a low reactivity fuel and resistant to compression ignition.

With emissions regulations becoming more and more stringent, more research has been focused on strategies such as HCCI and RCCI by using combinations of low and high reactivity fuels. Alkidas et al. have shown that HCCI can significantly reduce NO_X and soot emissions and fuel consumption, while HC emissions increased [16–18]. Common disadvantages are that HCCI methods have a regulated operating range due to rich/lean combustion based on fuel and a necessity for three-way catalyst after treatments [16]. These combustions methods produce high amounts of CO, HC, and NO_X emissions. Three-way catalysts use oxidation and reduction processes to convert these harmful emissions to CO_2, H_2O, N_2, and O_2. The greatest conversion efficiencies are achieved near stoichiometric operation, further limiting the operating range. In addition, Alkidas et al. found that HCCI has a strong dependency on chemical kinetics for the auto-ignition

combustion [16,17,19]. Aroonsrisopon et al. showed that lower octane fuels require leaner operating ranges, whereas higher octane fuels require more fuel rich operating ranges. They also showed that octane number is a poor indicator of combustion characteristics. Instead, fuel composition has a greater effect [20].

RCCI is a low temperature combustion variant of HCCI where both a low and high reactivity fuel are used. The low reactivity fuel is injected early to create a well-mixed charge, and then the high reactivity fuel is injected just prior to combustion of the mixed charge. This variability of injections allows for the optimization of the combustion phase, timing, and magnitude. Various fuels are used for RCCI, including gasoline, diesel, biodiesel, ethanol, regular fuels with cetane improvers, and many others. Reitz et al. have provided an extensive review on RCCI methods with various fuels, finding that RCCI has the potential to eliminate the need for NO_X and soot after treatments, while lowering exhaust gas recirculation (EGR) rates and increasing thermal efficiency [21].

2.2 Diesel Emissions Standards

Diesel engines have a wide range of emissions certifications. Each tier certification is dependent on the power rating of the engine and defines a maximum allowed combination of brake specific CO, HC, $NMHC+NO_X$, NO_X, and particulate matter (PM) emissions. From Tier 1 to Tier 4, CO, HC, $NMHC+NO_X$, NO_X, and PM emissions have seen reductions of up to 69%, 85%, 39% 96%, and 96%, respectively [22]. Other automotive emissions standards have seen similar reductions, and the precedent has been set for continued reductions out as far as 2025 [23]. For a John Deere 4045HF475 with Tier 2 emissions certification, the maximum CO, $NMHC+NO_X$, and PM emissions are 3.5,

6.6, and 0.2 g/kW-hr, respectively [22]. Dual fuel strategies aim to reduce these emissions with little to no sacrifice to engine performance.

2.3 Hydrous Ethanol Production

Ethanol in the U.S. is predominantly anhydrous, meaning all water content has been removed. Wang et al. showed that ethanol is produced by either a wet-mill or dry-mill process, where 80% of the ethanol plants in the U.S. use a dry-mill process [24]. A wet-mill process is more common when the desired coproducts are corn oil, gluten feed, and starch, in addition to the ethanol already being produced. The dry-mill process produces dried distiller's grains and solubles (DDGS), in addition to anhydrous ethanol.

Figures 3 and 4 depict the natural gas requirements to produce various concentrations of ethanol and the dry-mill process to produce anhydrous ethanol, respectively. Saffy et al. found that up to 46% of the total energy input can be accounted for from the distillation and dehydration processes alone [5]. By altering an existing plant, ethanol contents lower than 190 proof can be produced by installing a sectioned line during the distillation process. By reducing produced ethanol concentrations to 180 proof and removing the molecular sieve, the natural gas requirements can be reduced by 10%. These energy savings occur primarily in the stripping column and by removal of the dehydration stage. This removes the necessity to construct new plants, and lower ethanol concentrations can easily be produced. In addition, these energy savings make hydrous ethanol a more viable option as a secondary fuel.
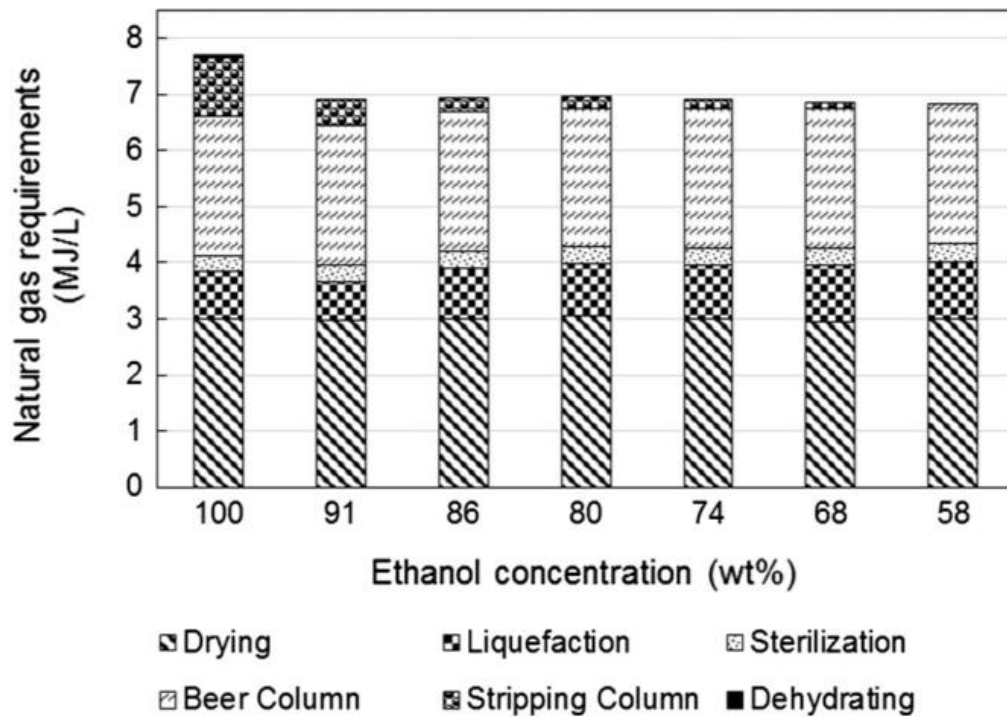
Figure 3: Energy requirement for production of various ethanol concentrations [5]
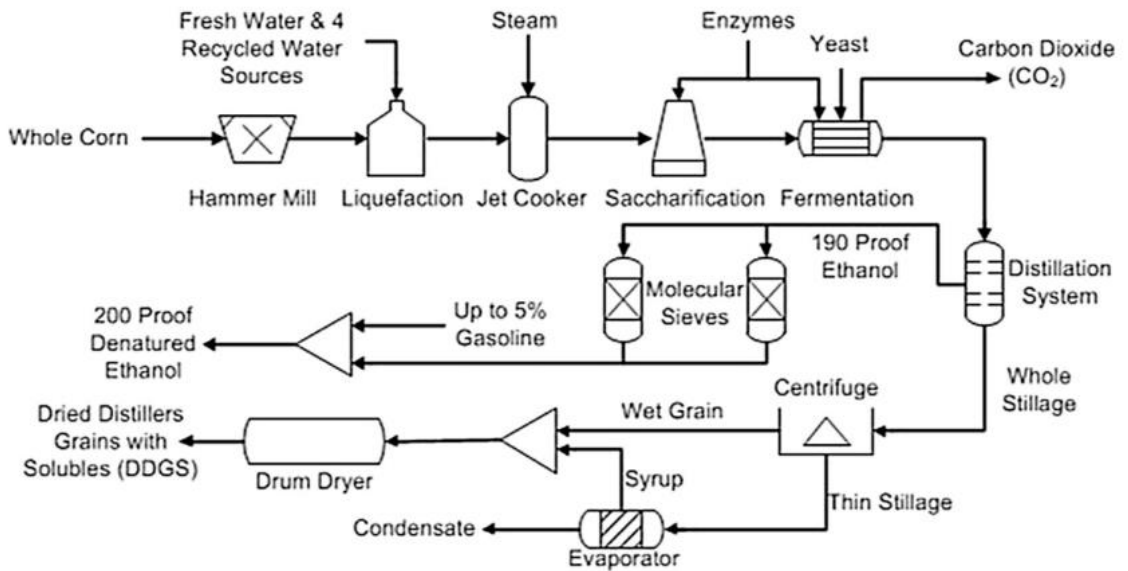
Figure 4: Dry-mill process for anhydrous ethanol production [5]

2.4 Dual Fuel Combustion

In hopes of meeting increasingly stringent emissions standards, aftermarket products have been developed to reduce emissions from legacy diesel engines. Particulate filters and diesel oxidation catalysts are some of the common options to help reduce harmful emissions such as NO, NO_2, HC, CO, CO_2, soot, and PM. Diesel oxidation catalysts work by oxidizing CO and HC with oxygen to create CO_2 and H_2O. NO_X emissions cannot be reduced during this process. Instead selective catalytic reduction (SCR) is used, where ammonia is introduced to help convert NO_X into N_2. To reduce soot concentration, diesel particulate filters are used. Particulate filters work by trapping soot particles until the exhaust back pressure reaches a specified level. A high temperature regenerative process is then used to oxidize the trapped soot, thereby clearing the filter and reducing the exhaust back pressure.

In addition to catalysts and filters, alternative fuels and dual-fuel strategies are being explored for their emission reductions with minimal sacrifice to engine performance and efficiency. RCCI, fumigation, and PFI strategies have been studied extensively, where a less reactive secondary fuel is used in conjunction with the direct injection of primary diesel fuel. These combinations have the potential to reduce NO_X and soot emissions while still obtaining high thermal efficiencies. Hydrous ethanol's resistance to auto ignition and water's dilution effect, reduces the need for EGR, making it an attractive fuel for dual-fuel strategies [25].

2.4.1 RCCI

Of the dual-fuel strategies commonly chosen, RCCI is desirable since it is known to yield high engine thermal efficiency. As explained above, RCCI utilizes two different reactivity fuels and a combination of injections to control the reactivity of the fuel being combusted. The low reactivity fuel is injected into the cylinder first to mix with air and recirculated exhaust gases and high reactivity fuel is injected prior to ignition. This allows for better control of the combustion phasing, magnitude, and duration [21].

In previous research, Dempsey et al. found an optimum mixture of 140 proof hydrous ethanol, where EGR was no longer necessary. Along with this finding, too much water in hydrous ethanol mixtures can lead to misfires from reduced flame speeds [26]. Fang et al. have shown that RCCI and 150 proof hydrous ethanol can achieve up to 75% FEF while achieving reductions in NO_X and soot emissions [25]. Although RCCI yields promising results, an original equipment manufacturer is often necessary for the modification, design, and calibration of engine components and controls, making this impractical for the aftermarket solutions market.

2.4.2 Fumigation

A more practical, marketable, and less invasive solution than RCCI is fumigation. This technique is more applicable to existing engines because stock diesel injection calibration can be left unaltered, however overall results have shown mixed success in terms of emissions reduction. Rahman et al. found it possible to use ethanol fumigation up to 40% FEF while retaining engine performance [27]. Alternative high reactivity fuels, such as canola biodiesel, showed decreases in PM, but only for low energy substitutions.

Excess ethanol, low cylinder temperatures, and unburned hydrocarbons were believed to have been the contributing factors leading to the oxidation of PM by OH radicals and in turn the reduction of PM overall.

In other studies that compared 20% FEF fumigation to emulsion blend methods, Abu-Qudais et al. found that the combustion behaviors were similar, but fumigation techniques produced more favorable emissions results. Increases in brake thermal efficiency (BTE), CO, and HC emissions, while decreases in soot emissions were also found through fumigation techniques in these studies [28,29]. In another study, Olson et al. compared 0, 100, and 200 proof hydrous ethanol fumigations, finding little sacrifice to BTE. As expected, HC emissions increased. Greater ethanol contents resulted in decreases in PM emissions, whereas greater water contents resulted in decreases to NO_X emissions [30]. Surawski et al. found that the vaporizing ethanol through the addition of a heat exchanger led to decreases in NO and PM emission whereas CO and HC increased, as compared to diesel only operation [31]. Hwang et al. implemented an aftermarket fumigation system on the same engine in a prior study. Using 120 proof hydrous ethanol, NO_X emissions and soot decreased with increasing FEF. On the other hand, CO and HC increased with increasing FEF [4]. Unfortunately, this system was only capable of producing FEF ranges of up to 10% due to poor mixing of air and fuel in the intake along with high water content hydrous ethanol requiring greater amounts of heat to help combustion. This, in turn, led to the design of a PFI system in hopes of producing greater FEF ranges and better vaporization of the hydrous ethanol being injected, potentially resulting in better mixing and combustion.

14

2.4.3 PFI

As stated previously, PFI used in dual fuel strategies has the potential to achieve greater levels for FEF through a more optimized fuel injection control and better vaporization of the PFI system itself. Hydrous ethanol is typically the secondary fuel of choice, but in some cases, using n-butanol as the secondary fuel has been explored. Soloiu et al. found lower soot concentrations and greater levels of unburned HC, when comparing PFI of n-butanol to n-butanol and neat diesel blends [32]. Few studies have been conducted examining the effects of PFI where hydrous ethanol is the secondary fuel. This study aimed to retain the original diesel calibration, while implementing a novel fuel rail and integrated heat exchanger for PFI of hydrous ethanol. The study test the hypothesis that that the addition of a heat exchanger to a hydrous ethanol PFI rail could enhance the vaporization of the ethanol. In turn, this would increase FEF capabilities and potentially lower the engine out emissions from a US-EPA Tier 2 certified engine. For this study, engine out emissions were reported as a function of FEF. Heated ethanol injection, unheated ethanol injection, and diesel only operation were each operated over eight standardized operating modes.

Chapter 3: Heat Exchanger Design

The concept of preheating the secondary fuel through the aid of a heat exchanger was investigated in this work. Initial plans sought to place a heat exchanger in series with the ethanol supply line to the PFI rail; however, a more compact system was desired. As a result, the innovative concept of combining both the PFI rail and the heat exchanger began.

3.1 Given Dimensions and Constraints

Detailed views of the given intake manifold and surrounding brackets can be seen in Figures 5, 6, and 7.
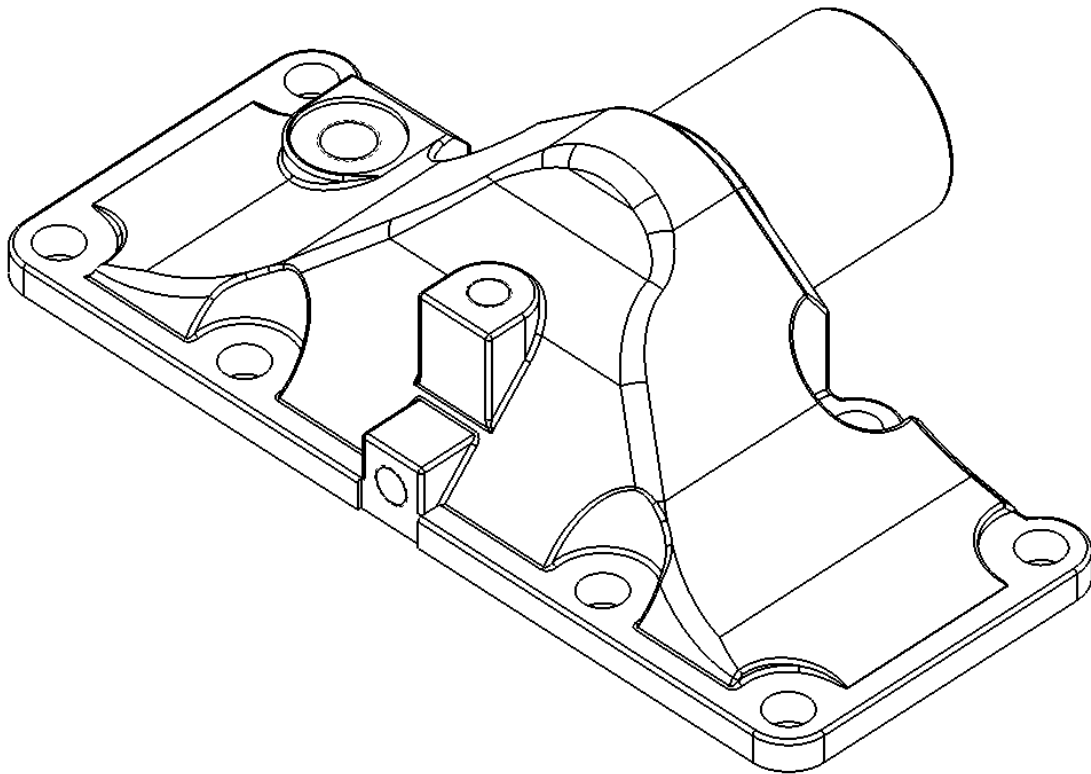

Figure 5: Isometric view of stock intake manifold
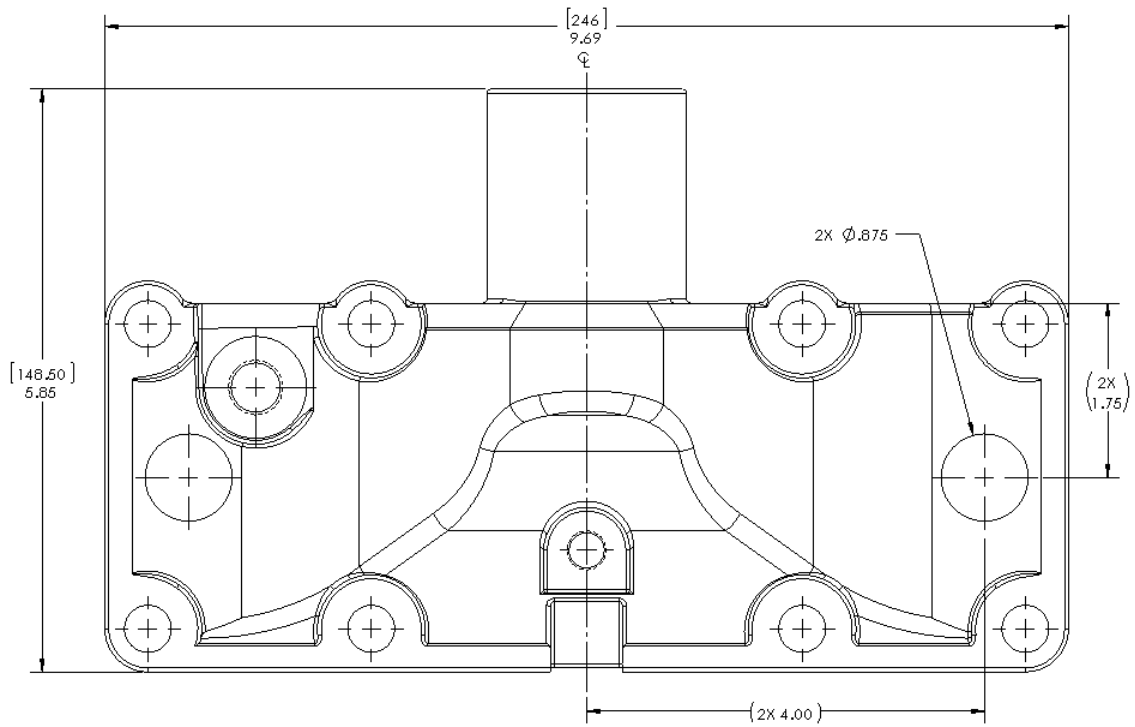
Figure 6: Front view and dimensions of modified intake manifold
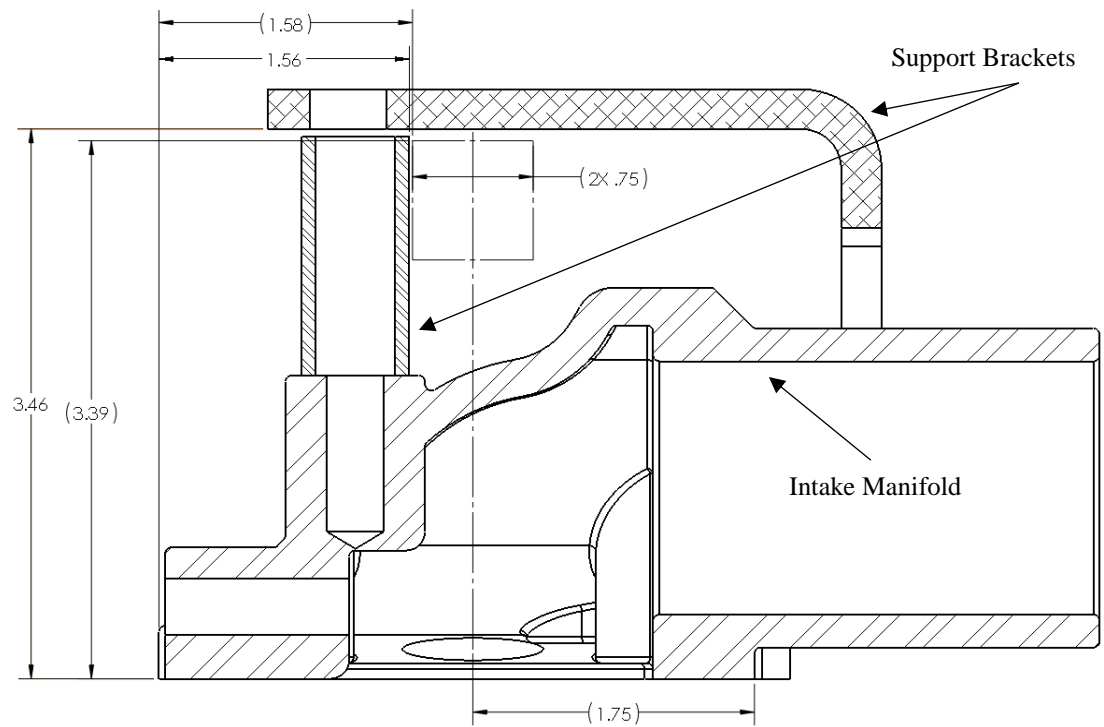
Figure 7: Section view and dimensions of modified intake manifold and supporting

brackets

Figure 6 shows a front view of the intake manifold to give a general idea of the maximum width placement of the ethanol injectors. This intake manifold was 9.69 inches wide. The injectors were placed 4.00 inches on each side of center and 1.75 inches back from the top flat face. Initially, it was planned that injectors would be placed at angles facing outwards towards each pair of cylinders to aid the fuel's path towards the back of the valves. Because of this possible angling, the injectors were placed 4.00 inches off center to reduce the slope of the intake manifold being machined. After further consideration, it was decided to place the injectors perpendicular to the intake manifold for ease of manufacturing and installation. Two 0.875 inch diameter holes were counter-bored into the intake manifold face. These were machined deep enough to provide enough support and area for welding of the injector bosses without altering the intake manifold's interface to the cylinder head.

Figure 7 details a centerline section view of Figure 6, where each bracket and the intake manifold are distinguished by separate cross-hatchings. A 0.75 x 0.75 inch square box can be seen where the body of the fuel rail was placed. With the surrounding support brackets, there was a 0.020 inch horizontal tolerance and a 0.070 inch vertical tolerance. Due to the height of the injectors and the bosses designed for the fuel rail, these tolerances were unavoidable.

3.2 Preliminary Designs

A shell and tube heat exchanger design was selected for the fuel rail design. The design process considered flow rates, inlet and outlet temperatures, pressure drops, physical properties, type of heat exchanger, line sizes and quantity, shell size constraints,

and materials for construction must be considered [33]. To optimize our design, a combination of SolidWorks and ANSYS were used to modify designs and compare subsequent performance. Note that the following subsections are not in chronological order, but instead describe the design processes that occurred for each section of the heat exchanger.

3.2.1 Heat Exchanger Shell Design

Initial designs for the shell of the heat exchanger considered using circular tubing. Swagelok T-fittings were going to be welded on to each end of the circular shell housing, as seen in Figures 8 and 9. To circulate the engine coolant, these T-fittings would have a singular internal tube connected to the outermost fittings. The outside fittings would circulate the engine coolant through the straight section of the T-fitting, and the ethanol inlet would be the perpendicular section of the T-fitting. From here, the ethanol would enter the T-fitting and circulate through the shell, around the coolant circulation line, and to the injectors. After considering additional fittings would need to be added to the shell for thermocouples, it was determined that a square shell would be more advantageous. A square shell allowed for slightly more room inside the shell, but more importantly it made the manufacturing process much easier. As a result, a 0.75 inch square tube with a 0.065 inch wall thickness was selected. The T-fittings were removed from the shell design and a separate chamber, on each end, was created to circulate the engine coolant. Each chamber were connected by a set of internal tubes, which are analyzed in the next subsection. Finally, the ethanol inlet was placed offset from the center for less interference with the stock mounting brackets surrounding the heat exchanger. A centered ethanol inlet resulted

in more counter-flow heat transfer as compared to co-flow. Offsetting the ethanol inlet to

the right also had the potential benefit of evening out each injection temperature.
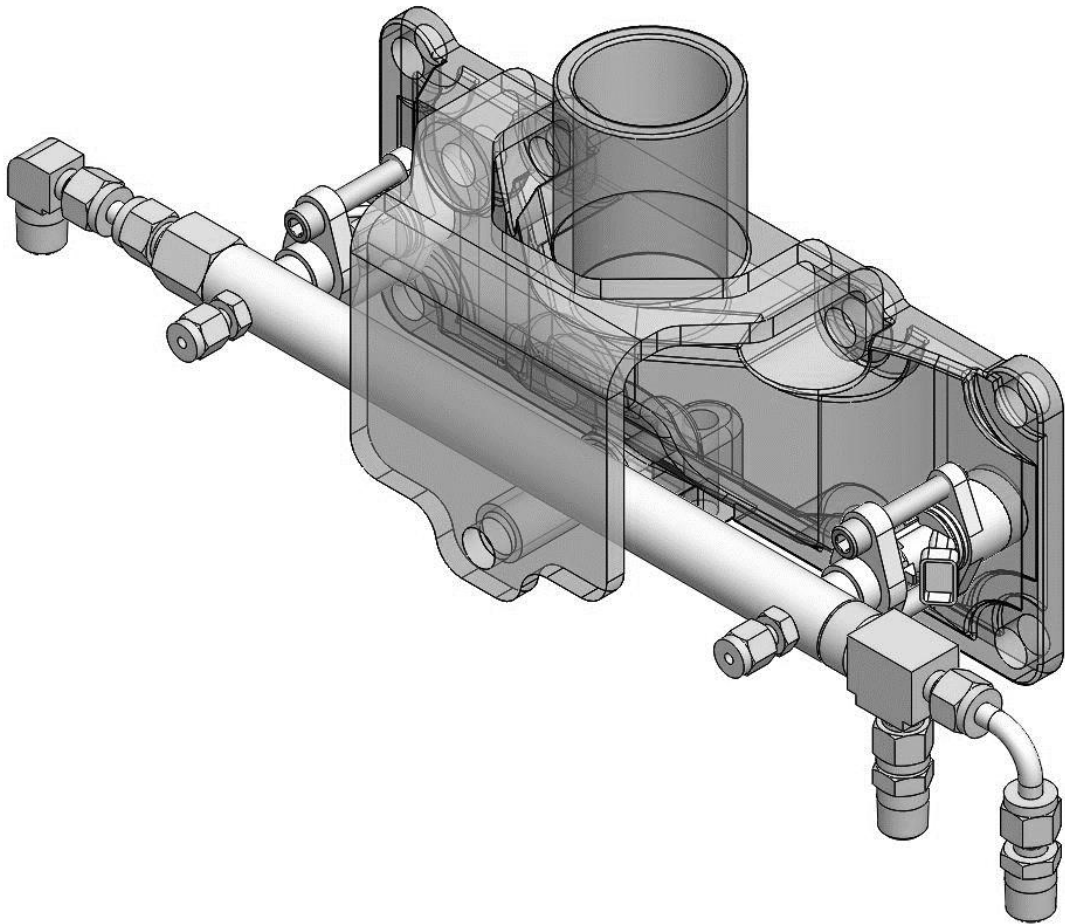
Figure 8: Isometric view of preliminarily designed, circular shell, heated fuel rail
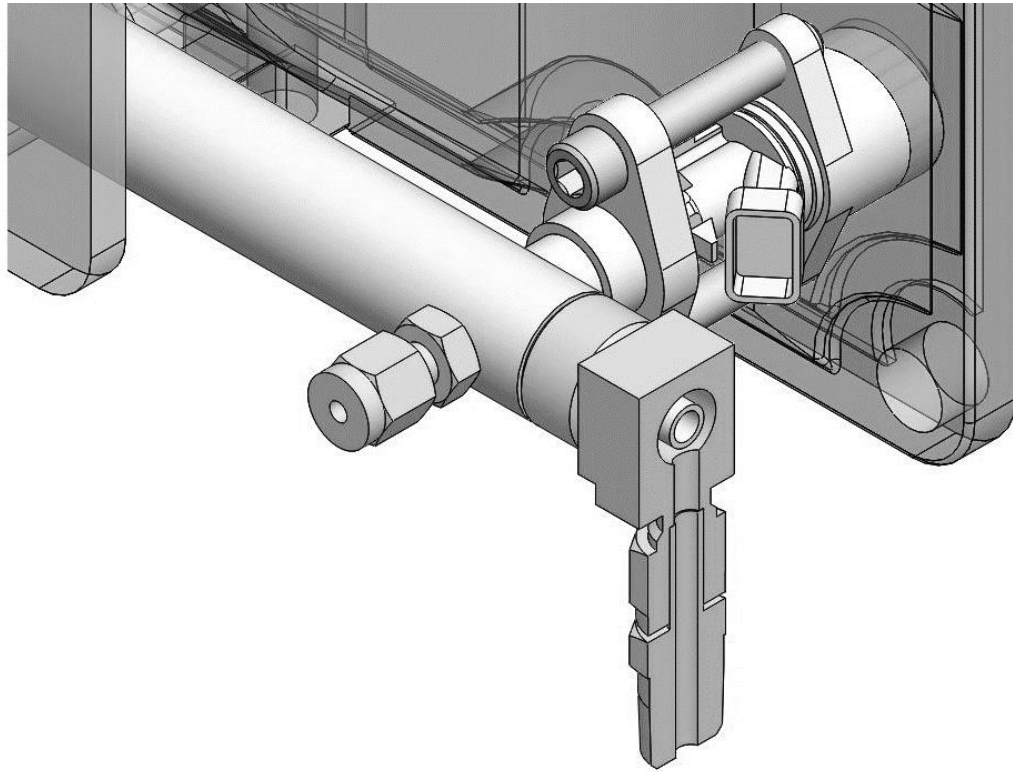
Figure 9: T-fitting section view of preliminarily designed, circular shell, heated fuel rail

3.2.2 Tubular Design and Quantity Analysis

For this portion of the heat exchanger design, the tubular section was analyzed. The quantity, diameter, wall thickness and arrangement were design considerations. At this point in the design process, a circular shell design was still selected and used when analyzing the tubular designs in ANSYS. Tube designs ranged from a single, 0.25 inch diameter tube running down the center, down to 25 0.0625 inch diameter tubes evenly spaced about a three ring arrangement. To determine the best configuration of tubes, ANSYS models were created and the mass flow average temperature was taken at each injector port. It was found that the 25 0.0625 inch diameter tube model would not converge

21

in ANSYS, leaving inconclusive results. Also, the packaging of the tubes in a very small space would have led to extremely difficult and unrealistic manufacturing conditions. From there, a single 0.50 inch diameter tube, and a triangular arrangement of three 0.25 inch and three 0.125 inch diameter tubes were explored. It was found that increasing the surface area significantly increased the amount of heat transfer, and as a result, the injection temperatures. It was also more advantageous to have a triangular layout of smaller tubes, rather than a single tube with a larger diameter. Triangular layouts have the potential to increase turbulence and therefore greater heat transfer coefficients [33].

3.2.3 Material Performance

Once the shell and tube design was finalized, the material was selected. Copper, aluminum, and stainless steel configurations were analyzed in ANSYS. Copper produced the greatest ethanol injection temperatures, followed by aluminum, and then stainless steel. The modeled results showed at most a 1.0°C difference between the materials. With that in mind, copper was eliminated to avoid soldering during the manufacturing process, and aluminum and stainless steel products were more available with the given constraints. Stainless steel, as compared to aluminum, was then found to show fewer corrosive characteristics when in the presence of ethanol [34–36]. With this, stainless steel was selected as the material for the manufacturing of the fuel rail and heat exchanger products

3.3 Final Design

After optimizing the shell, tube quantity and layout, and the material, a final design was chosen. Figure 10 shows the final design of the heat exchanger with a transparent view of the internal tubes and outer coolant circulation reservoirs. The optimum design was

determined to be a stainless steel, square shell model, with three tubes in an inverted, triangular layout. With this layout, engine coolant circulates from right to left, and thermocouples were placed on the shell opposite from the injector bosses where ethanol exits the heat exchanger. The ethanol inlet was offset to the right to eliminate the modification an existing support bracket. With a centered ethanol inlet, it was found that there were greater amounts of counter-flow heat transfer. Offsetting the ethanol inlet to the right would hopefully level out the difference between injection temperatures by decreasing the counter-flow heat transfer and increasing the co-flow heat transfer. After everything was optimized, top and bottom injector bosses were designed to accommodate the selected injector. Each boss is sized to match the ethanol outlet holes of the shell. Additionally, the insides are slightly undersized to allow compression of the injector O-rings and create a compression seal. Finally, each side has two fasteners that connect the top bosses and heat exchanger to the bottom bosses, ensuring the injectors are perpendicular to the intake manifold, the injector tips are exposed just past the inside wall of the intake manifold, and there is still easy access to the plug-in connection.
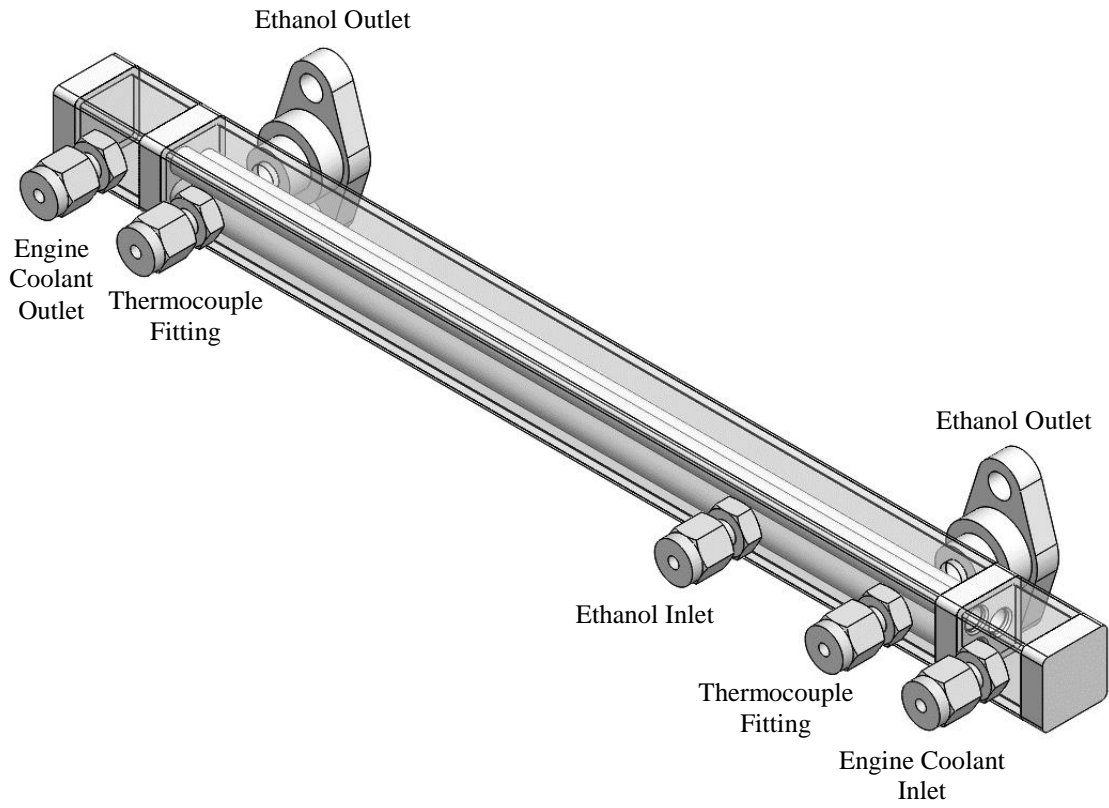
Figure 10: Final heat exchanger design with transparent sections

Chapter 4: Experimental Apparatus

4.1 Engine Specifications

A John Deere 4045HF475 Tier 2 diesel engine was used to conduct the dual fuel studies incorporating the designed fuel rail. The specifications of the engine and PFI system can be seen in Table 1, while the engine test setup can be seen in Figure 11.

Table 1: Engine Specifications

Manufacturer/Model	John Deere 4045HF475
Engine Type	4-Stroke DI Diesel
Cylinders	4, in-line
Displacement (L)	4.5
Bore x Stroke (mm)	106 x 127
Compression Ratio	17.0:1
Maximum Power (kW/RPM)	129/2400
Aspiration	Turbocharged & After Cooled
Diesel Injection System	Common Rail
Ethanol Injection System	Port Fuel Injection
Ethanol Heating System	Circulated Engine Coolant
Emissions Certification	EPA Tier 2 (Off-Highway)
EVO (CAD ATDCF)	120
EVC (CAD ATDCF)	380
IVO (CAD ATDCF)	339
IVC (CAD ATDCF)	567
PFI Pulse Widths (ms)	1-24
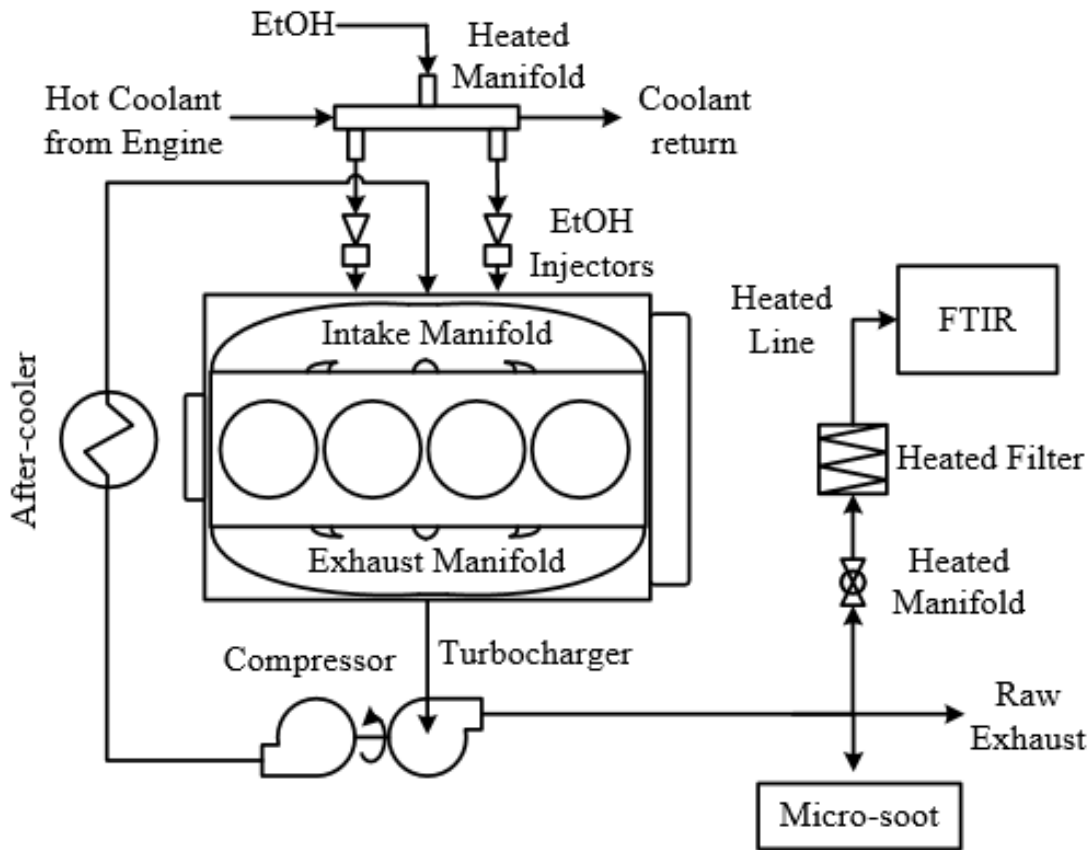
Figure 11: Diagram of engine test setup

The engine was equipped with thermocouples and pressure transducers at various locations to enable collection of the performance of various engine components. Specifically, the engine coolant, aftercooler outlet, and exhaust temperatures were measured to properly monitor the engine's behavior while providing realistic operating conditions when using ethanol dual fuel operation.

4.2 Intake Manifold Design

Looking specifically at the modified intake manifold design, a thermocouple was placed on the opposite side of the fuel rail from each injector inlet. This provided a good indication of the temperature of the fuel as it entered each injector. These temperatures are later analyzed and compared to the modeled results in the Performance chapter.
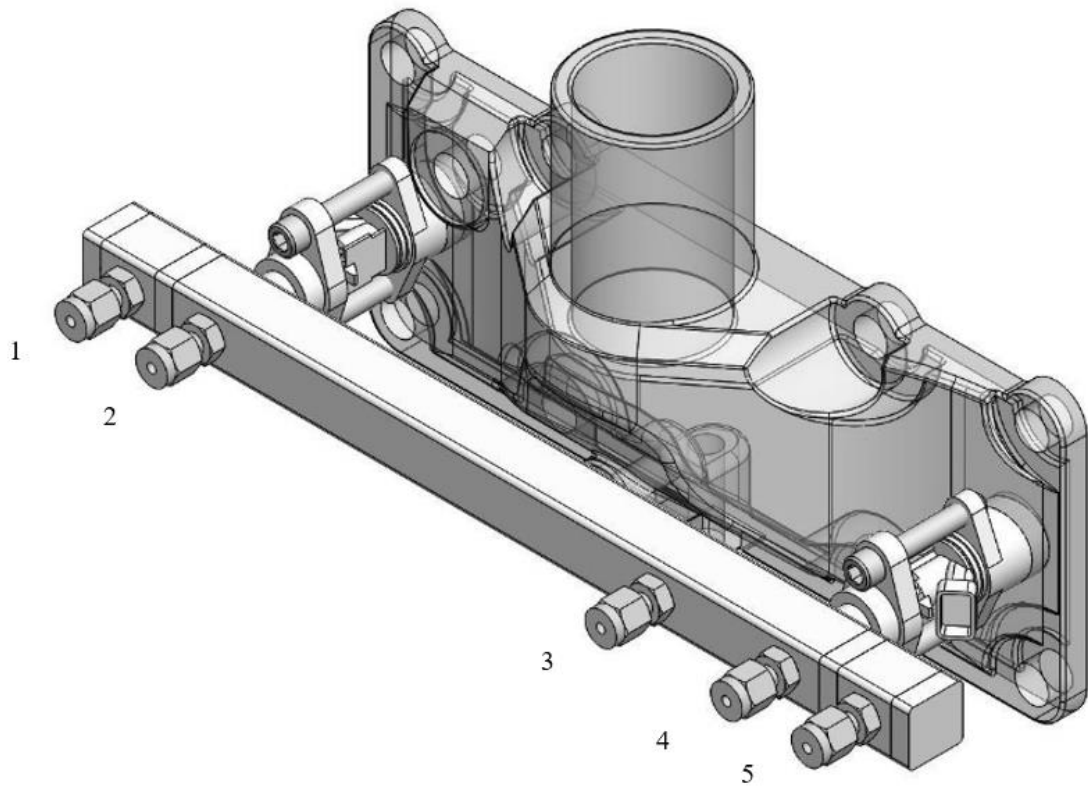
Figure 12: Isometric view of hydrous ethanol fuel injection system
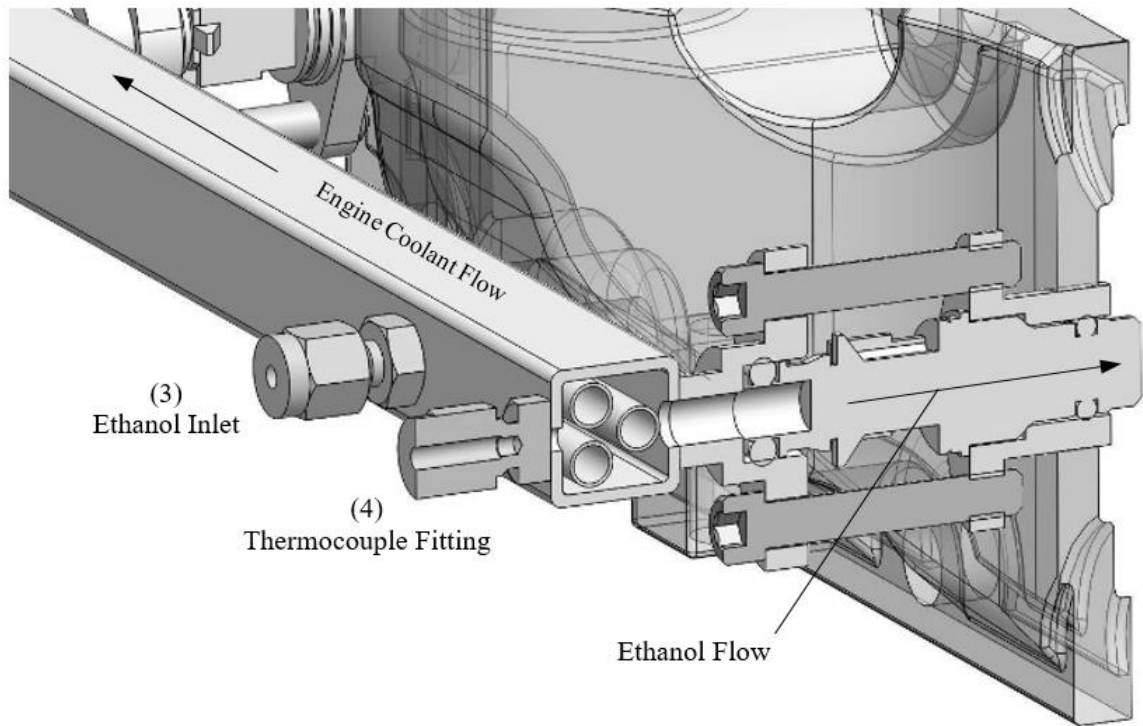
Figure 13: Injector section view of hydrous ethanol fuel injection system

To circulate the engine coolant through the tube portion of the shell and tube heat exchanger, hoses were connected upstream and downstream of the engine's thermostat. The upstream hose was connected to port 5, and downstream hose was connected to port 1, as seen in Figure 12. This setup creates a circulation from port 5 to port 1. Having the ethanol inlet offset closer to the engine coolant circulation inlet, results with less counter-flow and more co-flow heat transfer. For more detail, the ethanol and engine coolant flows can be seen in Figure 13.

Due to the length of the fuel rail being added to the intake, a custom water separator line had to be created to reduce interference. To reduce changes in the system, the same tube diameter, end fittings, and relatively the same length of tube were used to reroute the line.

4.3 Port-Fuel Injection

To control the port fuel injection, two 28 lb/hr Delphi 17113674 gasoline fuel injectors were selected and recessed past the inside wall of the intake manifold. The camshaft timing signal from the manufacturer-installed camshaft sensor was intercepted through a National Instruments (NI) LabView program and read using a NI cRIO controller. The camshaft timing signal provided both the engine speed and the location of cylinder 1 at top dead center (TDC). The NI program and controller then outputted the timing and pulse width to each injector.

The 180 proof (10% water by volume) hydrous ethanol was premixed in a secondary container prior to testing. This proof of ethanol was selected due to its lower distillation energy to LHV ratio from the refining process, and it does not require dehydration during its production [26]. During testing, it was sent from the container to the fuel rail at a relatively constant flow rate by use of fuel pump. This fuel pump maintained the ethanol fuel pressure between 60-100 PSI. The ethanol fuel flow rate was determined using a digital scale and collecting the differences in mass over each testing duration.

4.4 Engine Monitoring and Measurements

A laminar flow element (LFE) was used to determine the rate of intake air flow. An air-water heat exchanger was setup upstream of the intake to control the after-cooler temperature. To simulate actual operating conditions, the intake temperature was maintained in the range of 40-50°C. In addition, thermocouples were placed at various points of the engine for monitoring conditions and performance. More importantly, a thermocouple was placed in the coolant reservoir to not only monitor the engine's operating

temperatures, but also be used for an indication of the temperature of the engine coolant circulating to the heat exchanger on the PFI rail.

4.5 Emissions Measurements

An AVL Fourier Transform Infrared Spectrometer (FT-IR) was used to measure gaseous emissions and an AVL Micro-Soot Sensor (MSS) was used to measure soot mass concentration. Both instruments measured directly from the exhaust stack. The MSS operated with a built-in conditioning unit and dilution ratio of 10:1. This was necessary to help prevent instrument failure.

4.6 Methods of Data Collection

The test modes selected adhere to a modified 8 point steady state test plan in accordance with a type C1 off-road vehicle ISO 8178, as shown in Table 2 [37]. The engine load set points were lowered to match those used in our previous fumigation research, where the dynamometer resistor load banks were the limiting factor. The primary fuel was non-oxygenated #2 ultra-low sulfur diesel (ULSD) directly injected into the cylinder, and the secondary fuel was the 180 proof hydrous ethanol added through PFI.

Table 2: Engine operation conditions

Mode	Engine Speed (RPM)	Engine Load (N-m)	BMEP (bar)	Modified ISO 8178 Test Cycle	
1	2400	450	12.6	Rated Speed	90% Load
2	2400	350	9.77		70% Load
3	2400	250	6.98		50% Load
4	2400	50	1.40		10% Load
5	1400	450	12.6	Intermediate Speed	70% Load
6	1400	350	9.77		55% Load
7	1400	250	6.98		40% Load
8	1000	0	0.00	Idle	

To execute the test plan, the engine was allowed to warm and reach steady state prior to collection or altering the injection patterns. The engine speed and load were then set, where the dynamometer would control the engine speed and the throttle position adjusted the engine load. For PFI injections, the pulse width was set and injectors turned on. The engine speed and load were adjusted again to the parameters of the current test mode, and the system was allowed to reach steady state. Once steady state was reached, data was collected for five minutes at a rate of 1 Hz. Following data collection, the pulse width was then adjusted to the next setting and system adjusted to meet test mode specifications. This process was repeated across the range of pulse widths before changing test modes. For mode 4-8, the pulse width was increased until audible knocking was detected. The FEF range for modes 1-3 was limited due to the maximum flow rate of the injectors.

The same process was conducted for unheated ethanol PFI, in which case the engine coolant circulation valves were closed and cooled to ensure that no residual heat would be passed to the ethanol being injected. For diesel only operation, the engine coolant circulation valves were also closed to simulate standard engine operations. Error bars reported represent plus or minus one standard deviation of the data collected during each five-minute test period. These were calculated using the numerical sequential perturbation approach [38]. Error for the ethanol fuel flow was assumed to be equal to the resolution of the digital scale.

Chapter 5: Engine Performance and Emissions

5.1 ANSYS Model and Experimental Results

This section focuses on a comparison of the modeled and experimental results. Here the hydrous ethanol injection temperatures and the performance of the heat exchanger are examined.

5.1.1 Ethanol PFI Temperatures

Modeled and experimental results for the ethanol temperature, prior to injection, can be seen in Figure 14. Counter-Flow_Sim and Counter-Flow designate the right injector, which governs cylinders 1 and 2. Co-Flow_Sim and Co-Flow designate the left injector, which governs cylinders 3 and 4. Error bars were excluded because the experimental data was highly repeatable.

The modeled results showed a temperature range of 52-74°C, and the experimental results showed a temperature range of 46-79°C. Increasing the ethanol flow rate decreased the residence time in the fuel rail, and in turn led to the injector temperatures decreasing as well. Modes 1-7 had greater ethanol injection temperatures, as compared to mode 8. For modes 1-7, the engine coolant temperatures ranged from 78-85°C, and for mode 8, the engine coolant temperature was about 60°C. This difference in engine coolant temperature had a large effect on the injection temperatures due to the decreasing heat transfer while inside the heat exchanger. Looking at the separate injection temperatures, the co-flow side was consistently greater than the counter-flow side. The co-flow length is three times greater than the counter-flow length due to the offset ethanol inlet. By offsetting the ethanol

inlet, there was greater co-flow heat transfer than anticipated and resulted in uneven injection temperatures. The co-flow outlet temperatures ranged from 11-18°C greater than the counter-flow outlet temperatures for the modeled results and 8-14°C for the experimental results. These temperature differences showed an increasing trend with decreasing ethanol flow rate. Overall, the modeled temperatures were even with or slightly greater than the experimental results.
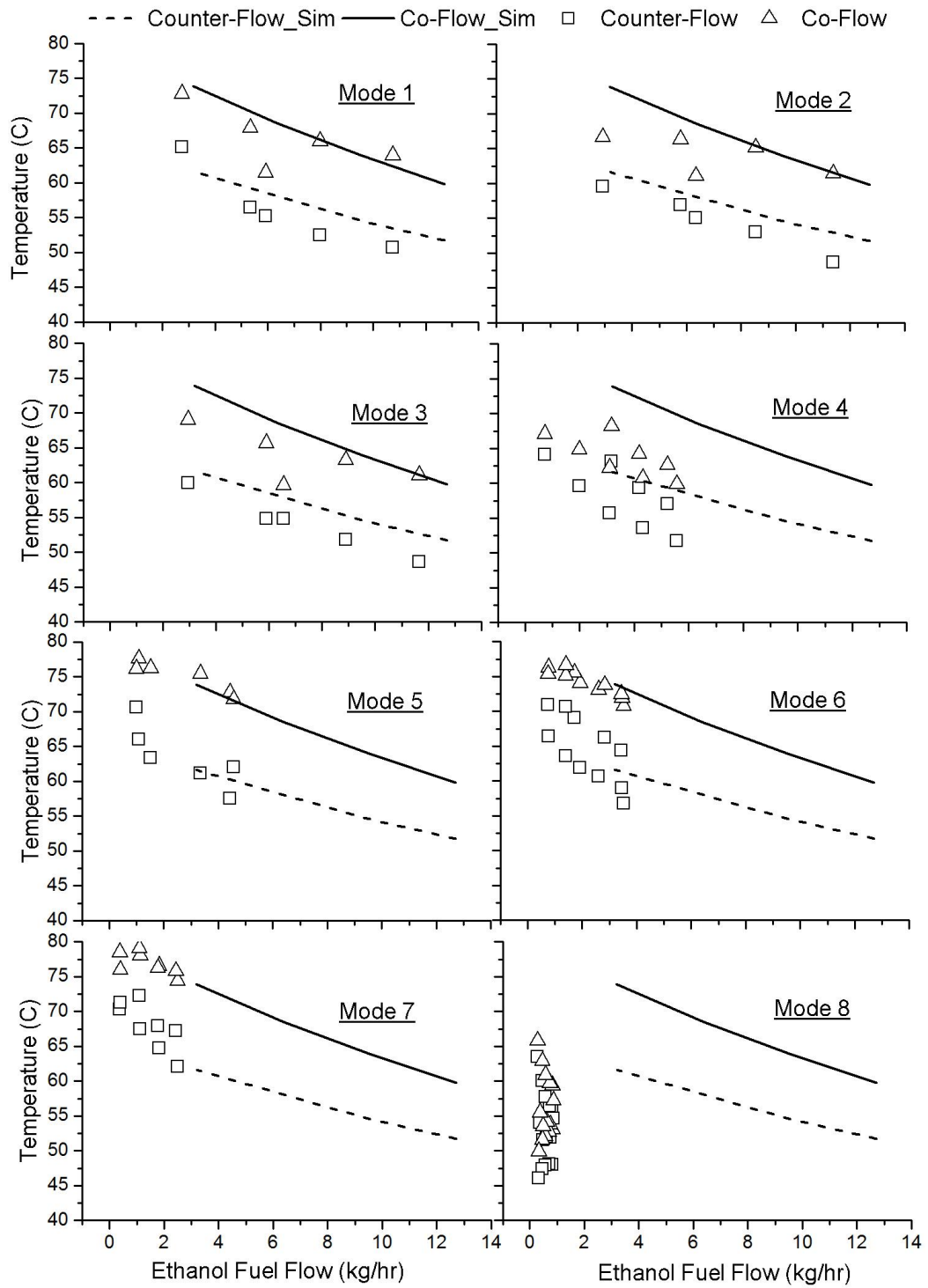
Figure 14: Simulation and experimental ethanol temperatures in °C as a function of ethanol fuel flow in kg/hr for each test mode

5.1.2 Heat Exchanger Performance

Various methods are used to examine heat exchanger performance. The log mean temperature difference (LMTD) method is often used to determine an adequate size of a heat exchanger based on a desired heat transfer rate and known inlet and outlet temperatures. The equation for determining the rate of heat transfer using the LMTD is shown in equation 1 below:

$$\dot{Q} = (UA)(CF)(LMTD) \tag{1}$$

Where:

- $\dot{Q}$ = Heat transfer rate (W)

- U = Heat transfer coefficient (W/m^2-°C)

- A = Heat transfer area (m^2)

- CF = Configuration correction factor (dimensionless)

- LMTD = Logarithmic Mean Temperature Difference (°C)

The configuration correction factor is used to account for geometrical deviations from true counter-flow heat transfer. This is determined by the arrangement of the shells and tubes along with the inlet and outlet temperatures of the fluids. Being that the ethanol heat exchanger system is very similar to a single pass heat exchanger, or dominantly counter-flow or co-flow, the configuration correction factor is equal to 1.00 [39]. By Tubular Exchanger Manufacturers Association (TEMA) standards, if considered as a single divided shell pass, single tube pass heat exchanger, the correction factor ranges between 0.99 and 1.00 [40]. It is a safe assumption to treat the correction factor as 1.00. The LMTD is then determined using equation 2.

$$LMTD = \frac{\left(T_{hot,in} - T_{cold,out}\right) - \left(T_{hot,out} - T_{cold,in}\right)}{ln\left(\frac{T_{hot,in} - T_{cold,out}}{T_{hot,out} - T_{cold,in}}\right)} \tag{2}$$

From temperature differences alone, the LMTD variable can often be used as an indicator of increasing or decreasing rates of heat transfer, as they are directly proportional.

The effectiveness-NTU method can also be used uses dimensionless parameters estimate heat exchanger performance. For this method, the effectiveness, ε, defined as the ratio of actual heat transfer rate to the maximum possible heat transfer rate, was determined using equation 3:

$$\varepsilon = \frac{\dot{Q}}{\dot{Q}_{max}} \tag{3}$$

Here the maximum heat transfer rate must be determined using the minimum heat capacity rate of the two fluids. The heat capacity rate for both cold and hot fluids are defined as:

$$C_{cold} = \dot{m}_{cold}C_{p,cold} \tag{4}$$

$$C_{hot} = \dot{m}_{hot}C_{p,hot} \tag{5}$$

Where:

- C = Heat capacity rate (W/°C)

- $\dot{m}$ = Mass flow rate (kg/s)

- C_p = Specific heat capacity (J/kg-°C)

For this heat exchanger, the heat transfer rate of the ethanol was examined. Looking at the results, the minimum heat capacity rate was that of the ethanol for each case, which simplified the equation for the effectiveness to:

$$\varepsilon = \frac{C_{cold}\left(T_{cold,out} - T_{cold,in}\right)}{C_{min}\left(T_{hot,in} - T_{cold,in}\right)} = \frac{\left(T_{cold,out} - T_{cold,in}\right)}{\left(T_{hot,in} - T_{cold,in}\right)} \qquad (6)$$

For the experimental results, the ethanol inlet temperatures and engine coolant outlet temperatures were unknown. To help simplify the calculations, the ethanol inlet temperatures were assumed to be 25°C. This assumption was used for the ANSYS models when designing the heat exchanger. For consistency and a more accurate comparison between modeled and experimental data, the assumption was kept the same. The modeled data also showed an average 1°C temperature drop of the circulated engine coolant across the range of ethanol flow rates. For consistency and a more accurate comparison as well, there was an assumed 1°C temperature drop of the circulated engine coolant for the experimental data. This was treated as a linear decrease along the coolant lines to help simplify the calculations for counter-flow, co-flow, and considering the offset ethanol inlet. In Figure 14, the temperatures detailed are those measured at the thermocouple locations. To properly determine the effectiveness and LMTD of the heat exchanger, the inlet and outlet temperatures of each fluid are needed. A correction factor of the difference between the modeled and experimental thermocouple temperatures was used to estimate the experimental ethanol outlet temperature. These estimated temperatures were then used in the calculations for the experimental effectiveness and LMTD.
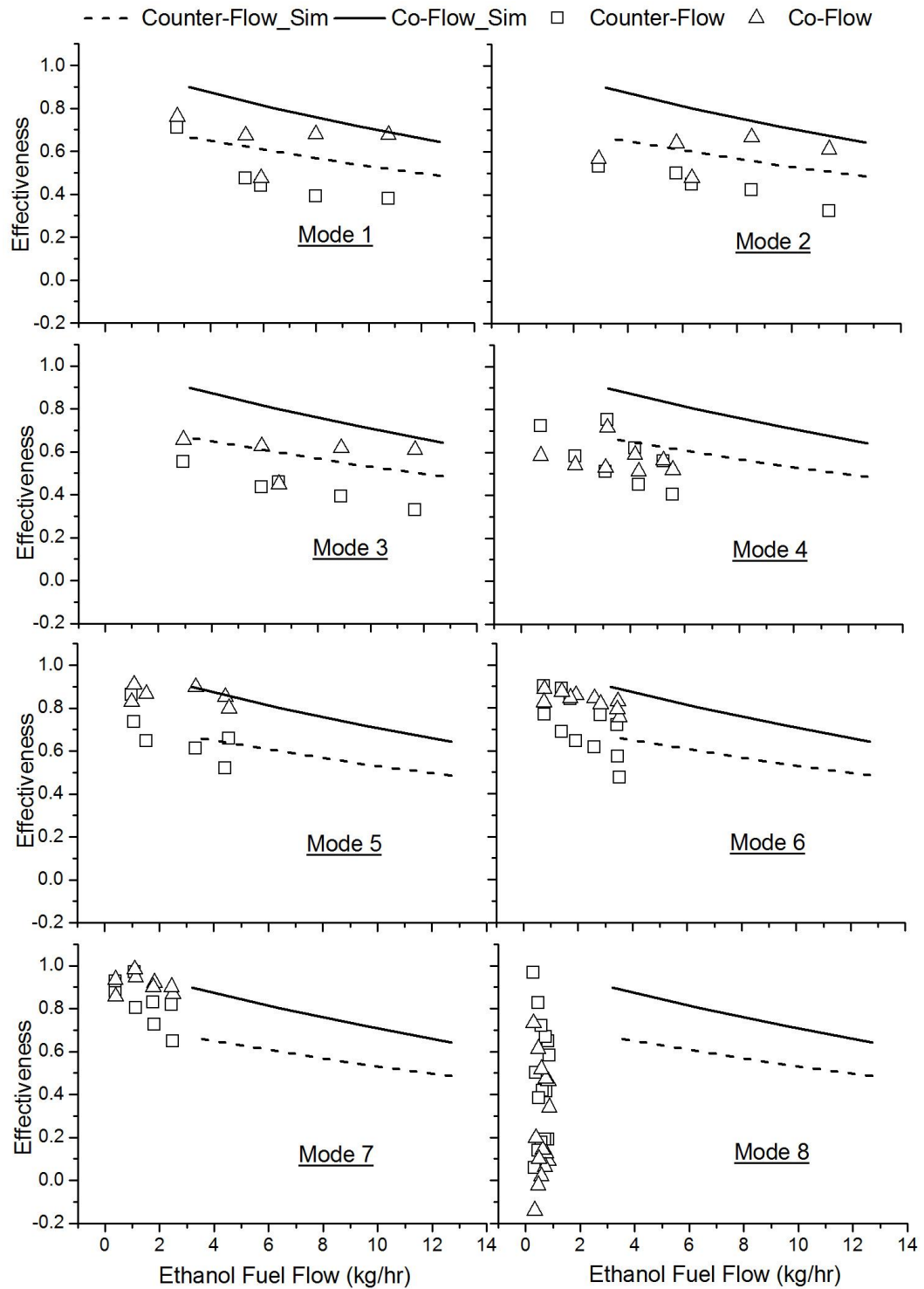
Figure 15: Simulation and experimental effectiveness as a function of ethanol fuel flow in kg/hr for each test mode

The effectiveness was calculated for both counter-flow and co-flow to examine the overall performance of the heat exchanger. Figure 15 details the modeled and experimental effectiveness. Error bars were left out due to the experimental error being very low. For each test mode, the experimental results followed a similar pattern to that of the modeled results where the effectiveness decreases with increasing ethanol flow rate. The experimental results also showed slightly worse performance than the modeled results. Modes 1-7 showed an effectiveness range of 0.32-0.98. For mode 8, the range of effectiveness is -0.14-0.97. Worth noting is that the experimental ethanol flow rates of mode 8 are extremely low at 0.288-0.864 kg/hr, in comparison to modes 1-7. Two co-flow effectiveness results showed a value less than 0.00. Effectiveness values less than 0.00 indicate that the ethanol outlet temperature was less than the inlet temperature. For these two instances, the room temperature may have been lower than the estimated inlet temperature of 25°C due to cooler ambient air being circulated through the test cell. During mode 8, the engine coolant temperatures only reached 59°C, whereas the average for modes 1-7 was about 82°C. Because there was less heat transfer and lower temperatures during mode 8, the ambient air may have had a greater effect than expected. Greater radiated exhaust temperatures near the engine coolant circulation lines may have caused an increase in the temperature of the circulated coolant lines and the ethanol being injected. This could have led to a discrepancy between the estimated 1°C decrease of the engine coolant inlet and outlet and as a result the negative effectiveness.

Along with the effectiveness, the LMTD was examined. For each mode, the LMTD showed an increasing trend with respect to the ethanol flow rate. This is an indication that

the overall heat transfer rate increased as the ethanol flow rate increased. A possible cause for this could be the increasing turbulence inside the shell of the heat exchanger as the flow rate increases. Note that the opposite trend is seen with the effectiveness and the injection temperatures. A simple explanation is illustrated in Figure 16 below, where the slope of the solid lines represents the rate of heat transfer and the ethanol flow rate. Note that the figure is not drawn to scale.

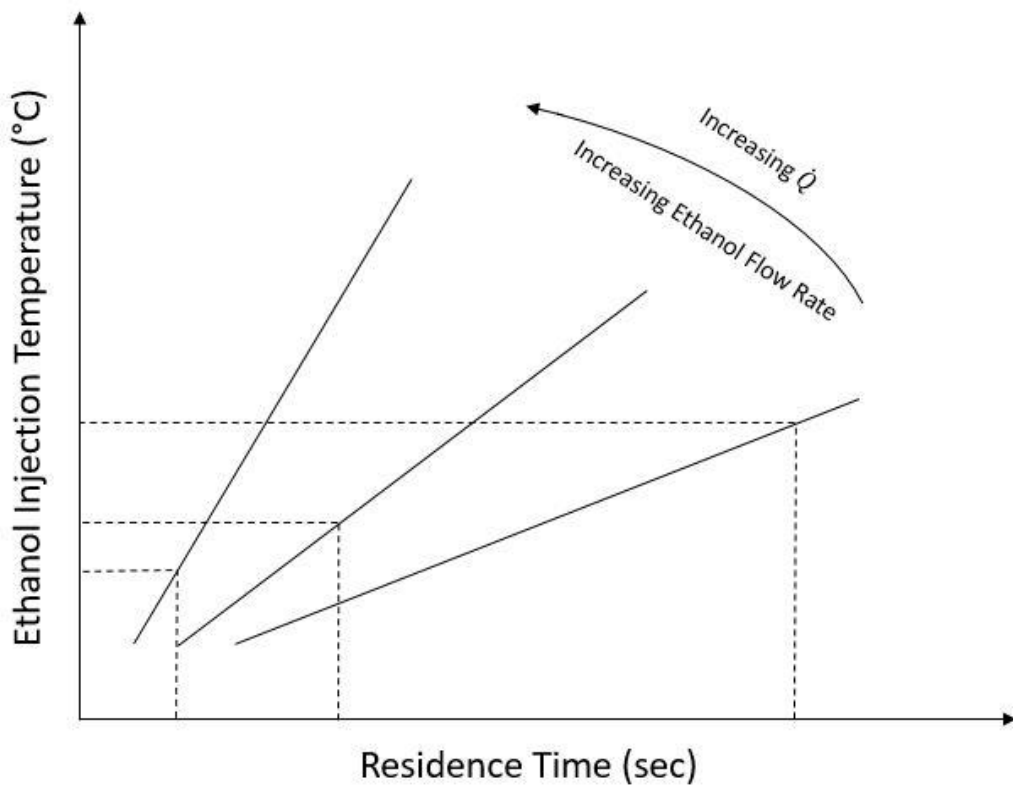**Figure 16: Illustrative figure of heat exchanger relationships**

It is intuitive to assume that as heat exchanger effectiveness increases, the ethanol injection temperatures and the rate of heat transfer would also increase. However, the rate of heat transfer performs the opposite. A likely reason for this is because the residence time decreases significantly enough to cause a decrease in the ethanol injection temperatures,

even though the rate of heat transfer increases. The heat exchanger itself is possibly sized poorly for this application; however, it still achieved adequate injection temperatures while still adhering to the design constraints. In future designs, the overall rate of heat transfer needs to be increased. A possible solution for this would be to add baffles between the ethanol inlet and each outlet. Another option would be to use tubes with enhanced surfaces. Both solutions aim to increase turbulence and decrease the potential buildup of a boundary layer. In the next section, the temperature profiles and path lines of the ethanol are explored for the current design.

5.1.3 Thermal Cross-sections and Ethanol Path Lines

Cross-sections of the heat exchanger, at high and low ethanol flow rates were created to examine its effect on the temperature profiles. Figures 17 and 18 detail the temperature profiles for 12.71 and 3.82 kg/hr ethanol flow rates, respectively. Looking at Figures 17 and 18, the ethanol's residence time in the heat exchanger has a large effect on the overall heat transfer. By decreasing the ethanol flow rate by 75%, the co-flow outlet temperature increased by 41.9%, and the counter-flow outlet temperature increased by 33.8%. Also, the time required to evacuate the internal volume of the heat exchanger increases from 8.1 to 32.3 seconds.
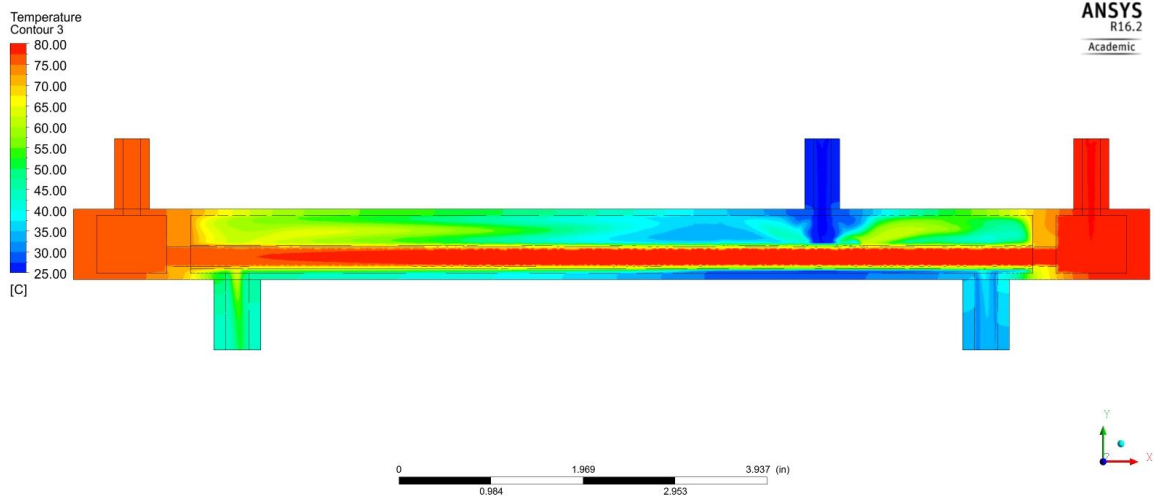
Figure 17: Thermal cross-section of the heat exchanger with an ethanol flow rate of

12.71 kg/hr
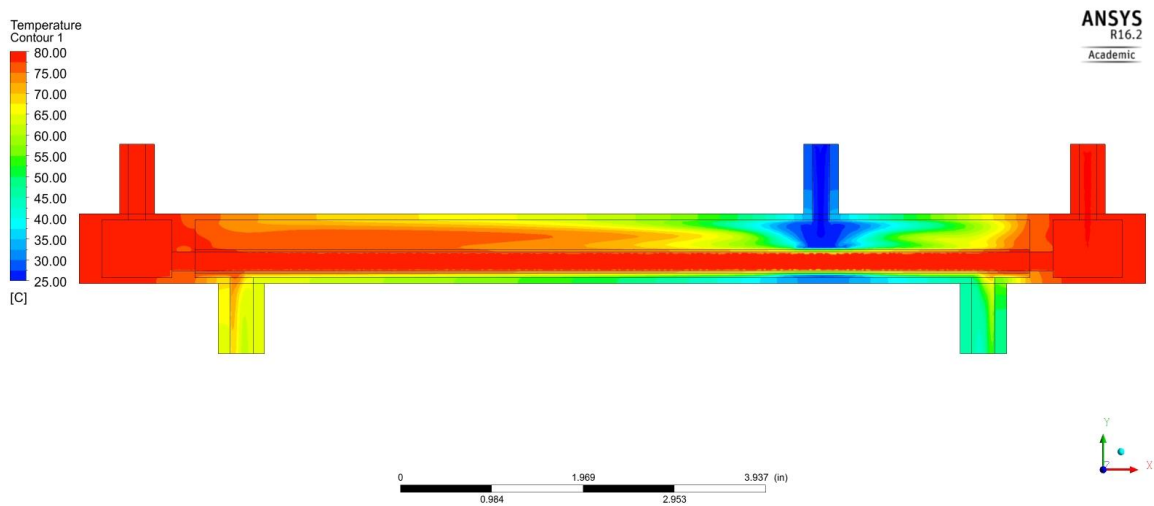
Figure 18: Thermal cross-section of the heat exchanger with an ethanol flow rate of

3.82 kg/hr

Velocity path lines of the ethanol inside the tubes can be seen in Figures 19-22.

Thermally and physically, the greater ethanol flow rate shows a large amount of turbulence

near the inlet, whereas the lower ethanol flow rate shows a smoother path line and thermal

profile. Conductive heat transfer occurs at the circulated engine coolant tube walls. A boundary layer can build up during laminar flow profiles, creating an insulating boundary layer and inhibits heat transfer. The maximum flow rate has an estimated Reynolds Number (Re) ranging from 250-3000, showing that most the path line is laminar. For a short distance at the ethanol inlet, the maximum velocity path lines enter a transitional Re regime but never achieve turbulent flow. Although the velocity increases enough to enter a transitional flow state, it is not for a long enough distance to significantly affect the overall heat transfer.
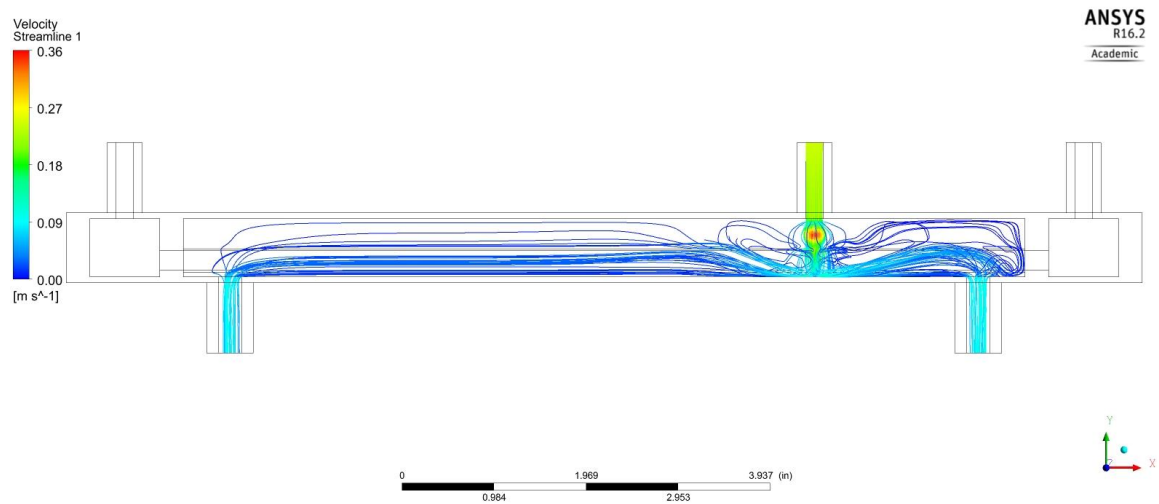
Figure 19: Front view of velocity streamlines for ethanol at a flow rate of 12.71 kg/hr
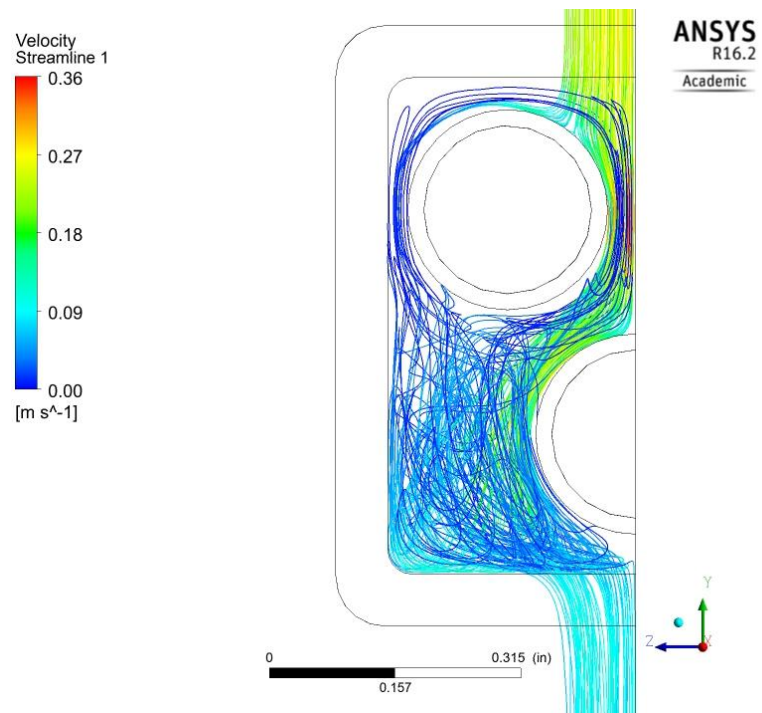
Figure 20: Right view of velocity streamlines for ethanol at a flow rate of 12.71 kg/hr
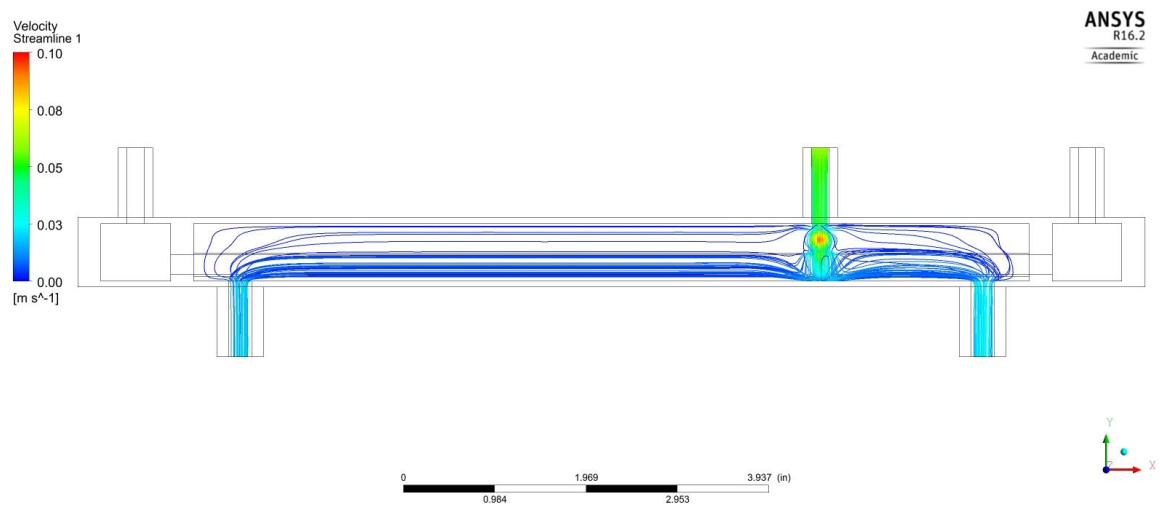
Figure 21: Front view of velocity streamlines for ethanol at a flow rate of 3.82 kg/hr
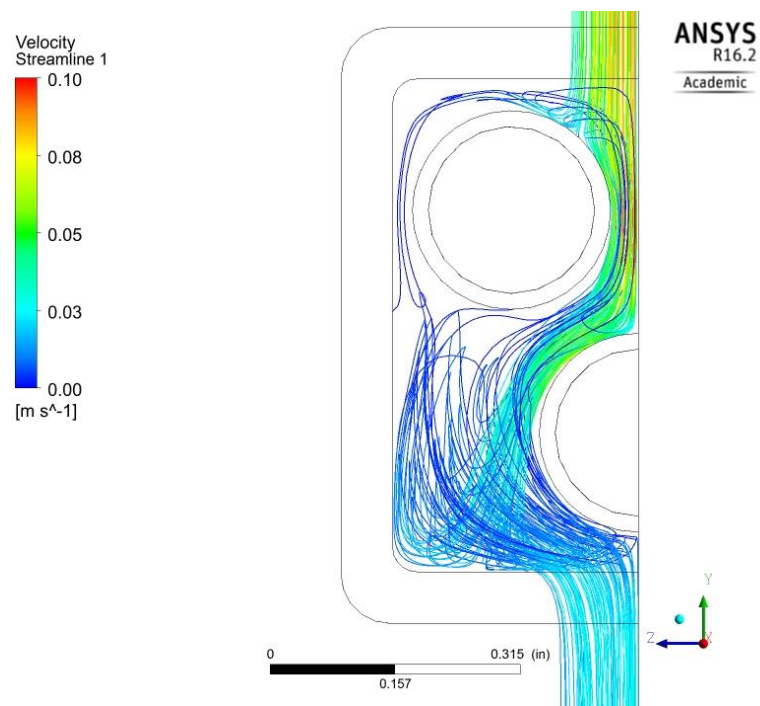
Figure 22: Right view of velocity streamlines for ethanol at a flow rate of 3.82 kg/hr

5.2 Engine Performance

In this section, the experimental results are analyzed and compared for each test mode and fuel injection type.

5.2.1 General Performance

The calculated brake mean effective pressure (BMEP), brake specific fuel consumption (BSFC), BTE, combustion efficiency (CE), air-fuel ratio (A/F Ratio), and FEF are given in Table 3. For each mode, the maximum FEF case for heated and unheated PFI was selected and compared to its corresponding diesel only operation. With respect to each diesel operation, BMEP remained relatively constant, BSFC increased, and BTE, CE, and A/F ratio decreased for all modes. A lack of combustion optimization and decreases in CE caused the decreases in BTE as FEF increased. Additionally, the decreases in CE led

45

to an increased amount of fuel necessary to maintain the same load, explaining the increased BSFC. As FEF increased, decreases in CE could have resulted from in-cylinder cooling, caused by the high latent heat of hydrous ethanol vaporization, along with increased amounts of water in the cylinder. Also, unburned ethanol is often trapped in the cylinder crevice volumes, contributing to the decreased CE and is a common occurrence in dual fuel methods.

Table 3: Engine performance over the eight test modes at the maximum fumigant energy fraction achieved

Mode	Operation	BMEP (bar)	BSFC (g/kW-hr)	BTE (%)	CE (%)	A/F Ratio	Max FEF (%)
1	Heated	12.6	315	31.5	96.2	20.9	18.9
	Unheated	12.6	327	30.8	96.0	20.2	20.9
	Diesel	12.6	226	37.9	99.8	29.7	0.00
2	Heated	9.77	347	29.8	95.4	20.3	24.4
	Unheated	9.79	365	28.9	95.5	19.1	27.3
	Diesel	9.71	236	36.4	99.7	32.2	0.00
3	Heated	7.06	393	27.7	94.3	20.6	32.2
	Unheated	6.94	442	25.1	94.1	19.4	34.8
	Diesel	6.91	249	34.5	99.5	35.6	0.00
4	Heated	1.41	856	13.1	93.3	34.6	36.4
	Unheated	1.40	856	13.1	93.1	34.0	37.2
	Diesel	1.34	432	19.9	98.5	70.0	0.00
5	Heated	12.4	280	34.6	98.7	16.7	15.3
	Unheated	12.5	275	34.7	98.8	17.0	13.4
	Diesel	12.5	207	41.4	99.4	22.4	0.00
6	Heated	9.90	277	34.8	98.4	18.5	14.9
	Unheated	9.76	283	34.2	98.6	18.5	15.3
	Diesel	9.71	216	39.7	99.7	24.5	0.00
7	Heated	6.94	295	32.5	97.8	22.0	14.1
	Unheated	6.94	288	33.4	97.9	22.4	14.7
	Diesel	6.92	223	38.4	99.7	29.5	0.00
8	Heated	0.740	770	13.7	94.8	67.8	27.0
	Unheated	0.787	734	14.3	95.1	66.3	26.9
	Diesel	0.615	531	16.1	98.6	115	0.00

5.2.2 FEF Results

The maximum FEF achieved across each test mode can be seen in Figure 23. Modes 1-3 were limited by the flow capacity of the injectors. Modes 4-8 were limited by the onset of knock, which was determined audibly. Looking at each mode, unheated ethanol PFI allowed higher FEF than heated ethanol PFI. Greater ethanol temperatures caused the density of the fluid to decrease. With the pressure and injection duration remaining constant, the same volume was injected resulting in a lower mass flow rate. Modes 1-3 were limited by the injector flow rate. Mode 4 achieved the greatest FEF as the mode was the lowest load at high engine speed tested. The low load and high-speed combination allowed for a large achievable FEF without being limited by the injector's capabilities. Modes 5-7 were high load, low speed cases and showed a distinct limitation of 15% FEF where knock was apparent. This limitation marks a distinct barrier of diesel replacement strategies at lower engine speeds.
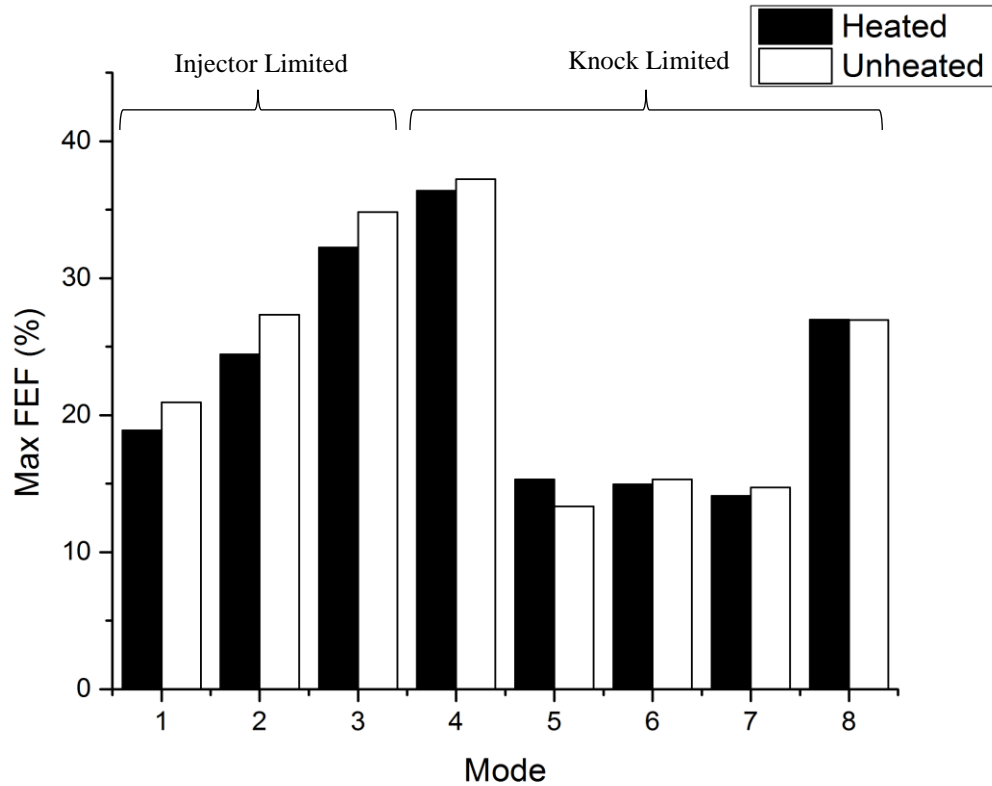
Figure 23: Maximum FEF achieved for each test mode for heated and unheated ethanol injection

5.3 Engine Emissions

An AVL FT-IR and MSS were used to collect engine emissions data. NO, NO_2, NO_X, CO, total hydrocarbons (THC), ethanol, and soot emissions were collected for both heated and unheated ethanol injections and compared to diesel only emissions. All emissions, except soot, are reported with brake specific units. Soot emissions are reported in density units of mg/m^3.

5.3.1 NO Emissions
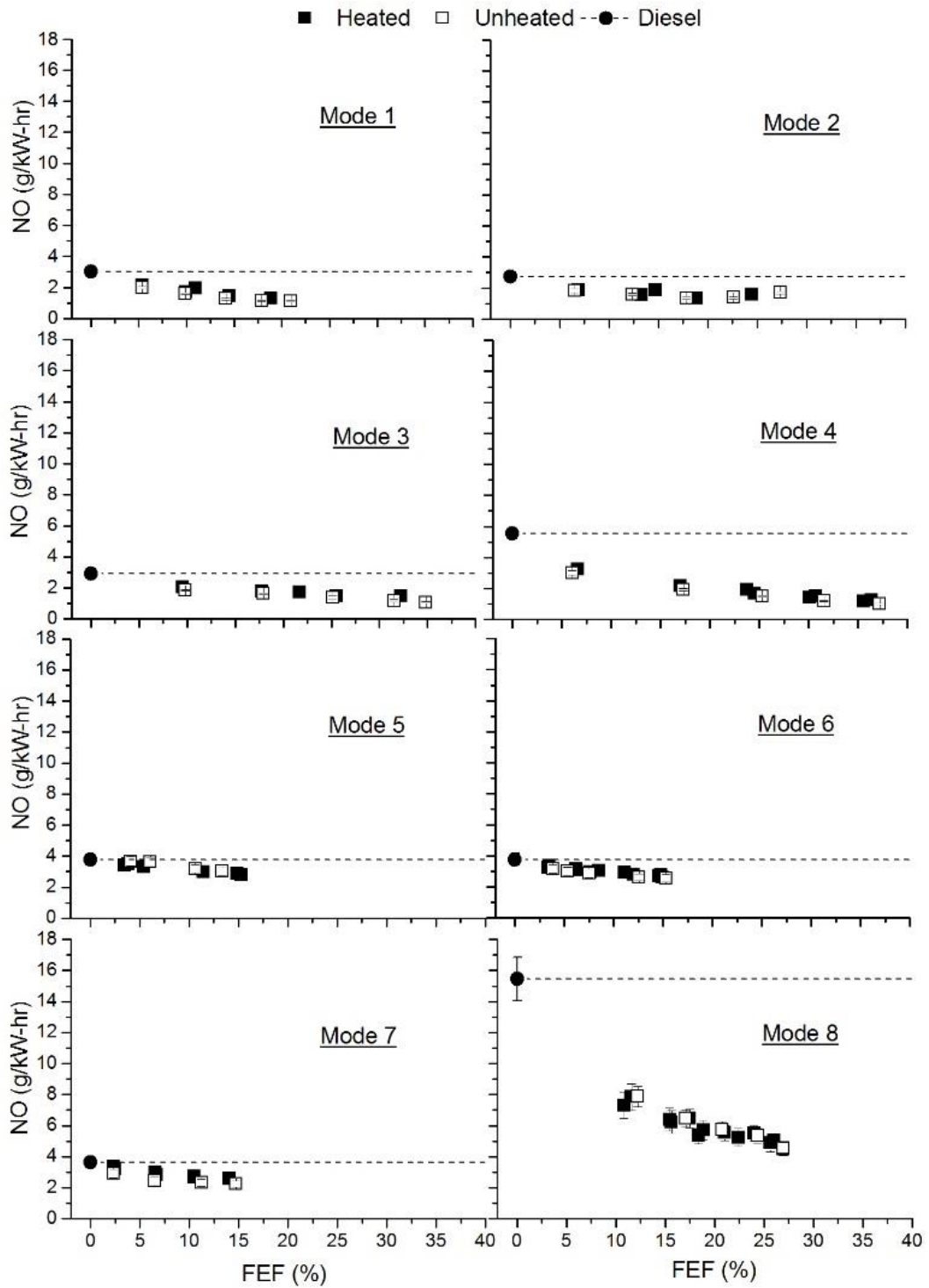
Figure 24: Brake-specific NO emissions as measured by FT-IR in g/kW-hr for each

mode as a function of FEF

Reducing NO_X emissions is a primary reason commonly given for implementing dual-fuel strategies in CI engines. NO_X consists of NO and NO_2. Water injection is well known to reduce NO formation [41]. Consistent with our findings, Hulwan et al. found that lower in-cylinder temperatures, caused by the higher latent heat of ethanol vaporization, decrease NO formation when using dual-fuel ethanol fumigation. The same trend was also explained by increased ignition delays, caused by lower cetane numbers [42]. Figure 24 shows brake-specific NO emissions as a function of FEF, for each test mode. The horizontal, dotted line corresponds to each mode's diesel only operation at 0% FEF. For each case, NO emissions decreased as FEF increased. This was expected due to the lower global cylinder temperatures. Comparing heated and unheated ethanol PFI, heated PFI would be expected to have greater NO emissions due to higher temperatures at the intake valve closing event; however, there were no significant differences in NO emissions between the two operating conditions as a function of FEF.
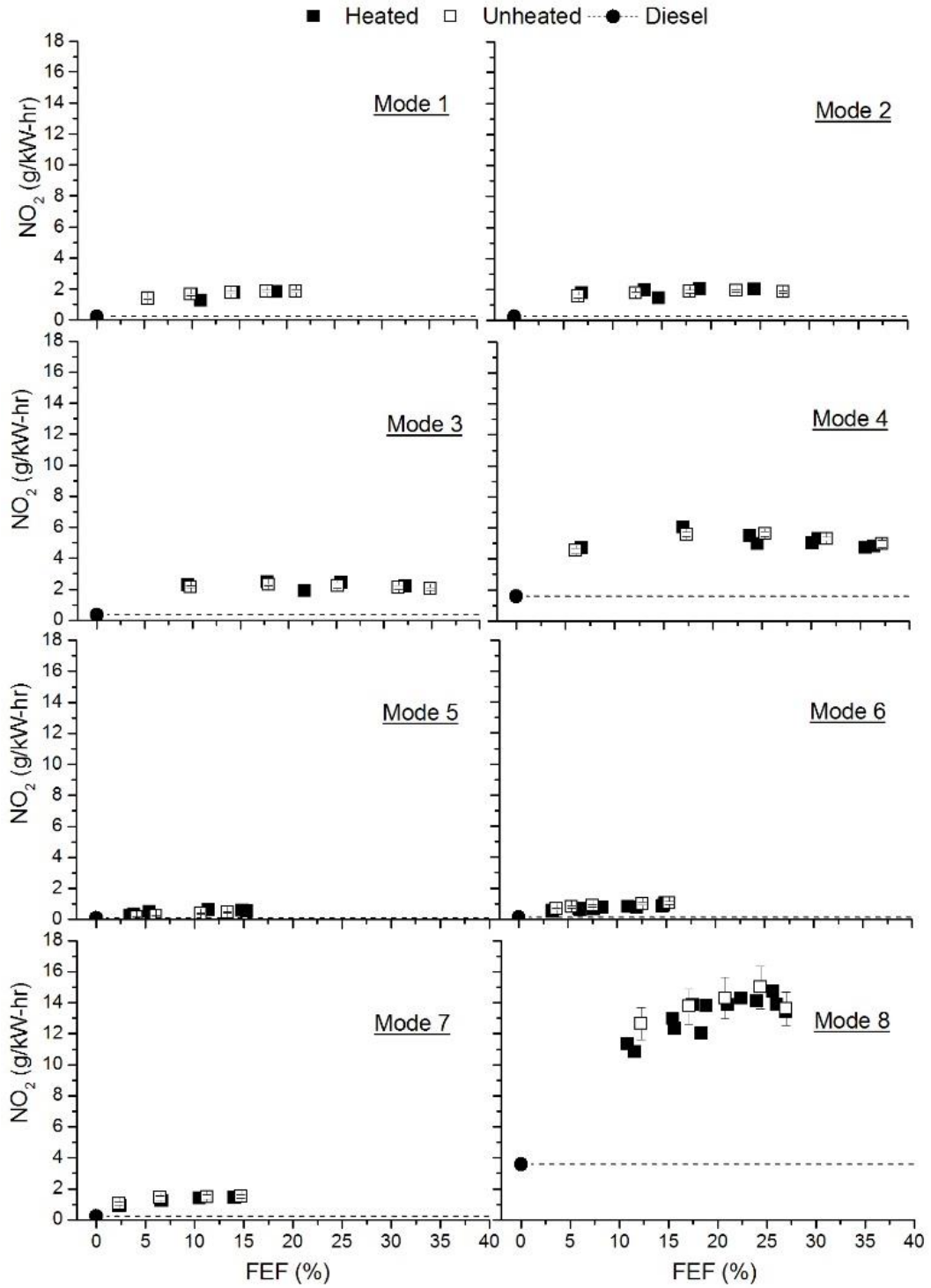
5.3.2 NO₂ Emissions

Figure 25: Brake-specific NO₂ emissions as measured by FT-IR in g/kW-hr for each mode as a function of FEF

Brake specific NO_2 emissions are reported in Figure 25. Although NO emissions decreased with increasing FEF, NO_2 increased. Others have shown that HO_2 radicals are primarily responsible for the conversion of NO to NO_2 when excessive hydrocarbons are present, like in dual fuel combustion modes[43,44]. At higher temperatures, HO_2 becomes unstable, hindering its ability to react with NO, leading to greater NO emissions and less conversion to NO_2. With lower combustion temperatures, the HO_2 radical becomes more stable, promoting conversions to NO_2. Bika et al. have shown that increases in H atom concentrations during combustion promote the formation of HO_2 [45], whereas Bowman found that even low concentrations of HC can aid the conversions of NO to NO_2 [43]. Hori et al. explored the influence of hydrocarbons on the conversion of NO to NO_2. They found that ethylene and propane were very successful, but methane and ethane had a lesser tendency for conversion [46]. Hwang et al. found that for ethanol, unburned HC increase with FEF and facilitate the conversion of NO to NO_2, particularly in the temperature range of 800-1200 K, which was likely experienced during the expansion stroke. For in-cylinder temperatures above 1400 K, ethanol is assumed to become fully converted as there is no more conversion from NO to NO_2, and for temperatures below 1150 K, less OH radicals are present and limit the production of HO_2. Both of these temperature limits clearly prevent the conversion of NO to NO_2 [47]. Our results showed that ethylene and methane are the most prominent unburned HC and increase with FEF. Overall our findings on the conversion of NO to NO_2 can be explained by the abundance of unburned ethanol from combustion increasing the H atom concentration and therefore HO_2.

Aftertreatment methods have been shown helpful with reducing NO_2 emissions. Selective catalytic reduction (SCR) aftertreatment is commonly used in modern diesel engines. Kittelson et al. [48] and others have shown that SCR is optimal for reducing NO_2 levels when the molar NO_2/NO ratio approaches a value of 1.0. Modes 4-8 showed increases in FEF increased the NO_2/NO ratio. For Modes 4 and 8, NO_2/NO started at about 1.5 and increased to 3.8 and 3.0, respectively. For Modes 5, 6, and 7, this ratio increased from 0.07 to 2.0, from 0.14 to 0.39, and from 0.28 to 0.56, respectively. Modes 1-3 showed varied results. The NO_2/NO ratio starts below 1 for low FEF and continues to rise past a ratio of 1 for higher FEF. These trends show that SCR would be optimal for reducing NO_2 emissions for high load conditions only. Overall increases in FEF are more beneficial at low engine speeds. For higher engine speeds, low to mid-range FEF's are most beneficial.

5.3.3 NO_X Emissions

NO_X emissions are largely dependent on local combustion temperatures and residence times in the cylinder because the Zel'dovich mechanism is rate limited at engine-relevant timescales. Looking at Figure 26, the NO_X emissions remain relatively constant across each range of FEF for each test mode, showing that the cylinder temperatures had a much greater effect than expected on the NO and NO_2 emissions. As stated previously, NO emissions decreased, whereas NO_2 emission increased. Seeing that NO_X remains constant, the increases in NO_2 are likely coming from the stabilization of the HO_2 radical, from lower cylinder temperatures, and greater H atom concentrations helping promote the conversion on NO to NO_2. This shows that the same amount of NO_X emissions are being produced, as compared to diesel only operation, and that only NO and NO_2 were being affected.
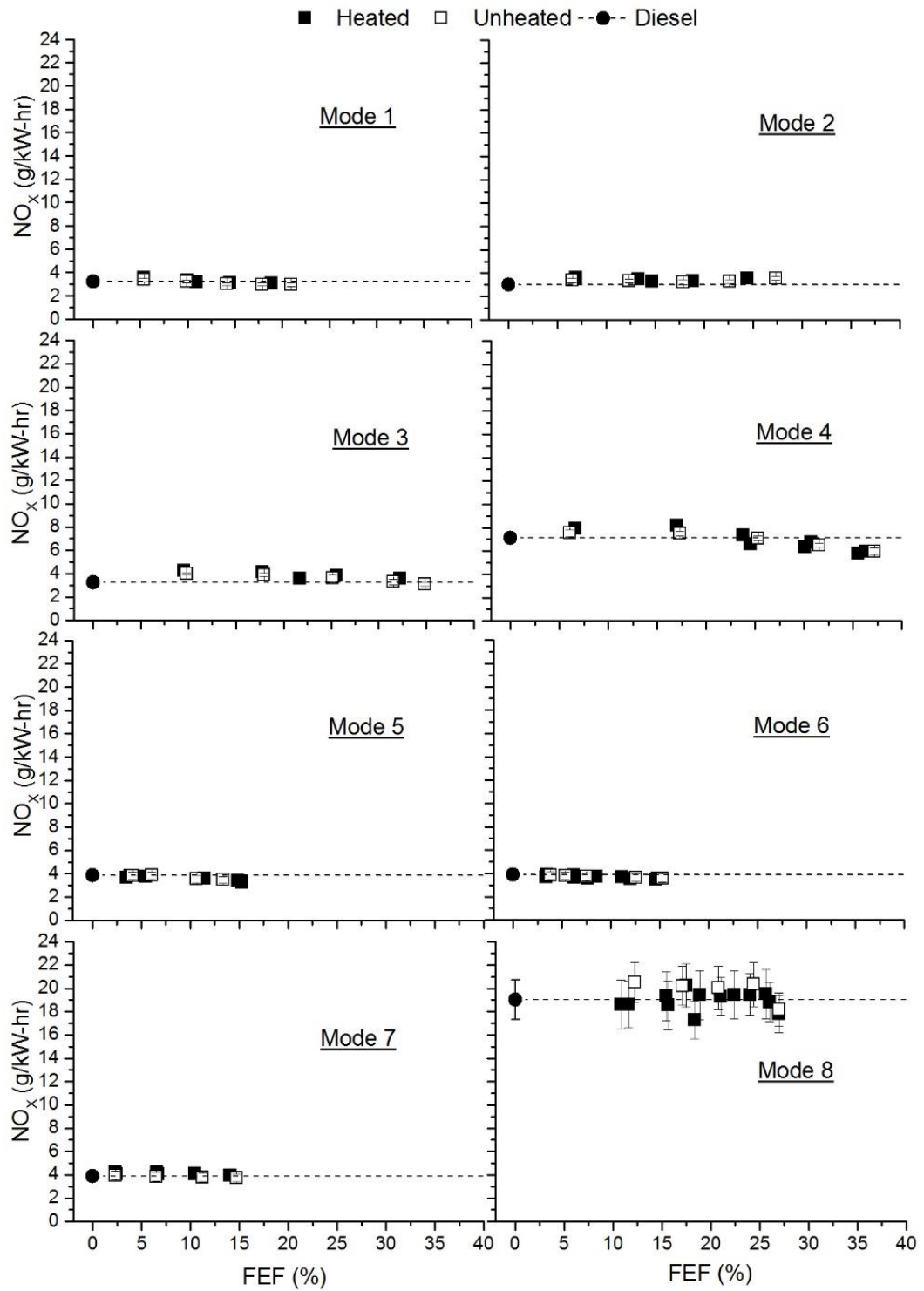
53

Figure 26: Brake-specific NOₓ emissions as measured by FT-IR in g/kW-hr for each

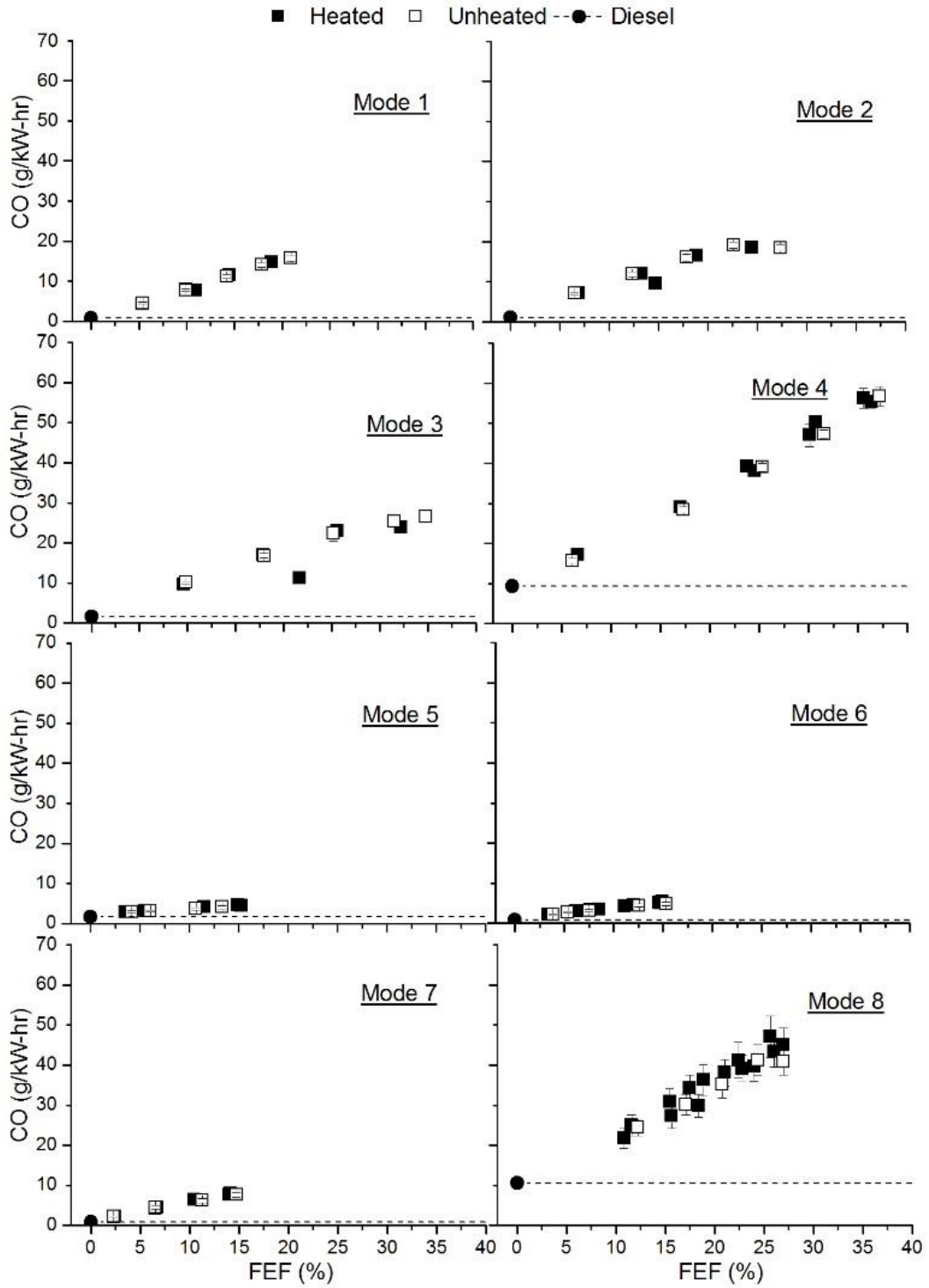**mode as a function of FEF**

5.3.4 CO Emissions

Figure 27: Brake-specific CO emissions as measured by FT-IR in g/kW-hr for each

mode as a function of FEF

Figure 27 details the brake specific CO emissions for heated and unheated ethanol injection across each range of FEF for each test mode. CO emissions increased as a function of FEF with little to no distinction between heated and unheated ethanol injection. The increases in CO emissions are seen to be associated with increased ethanol fuel flow. The increases in CO emissions seen in these results may have been caused by decreasing in-cylinder temperatures, with respect to FEF, causing the incomplete oxidation of CO to CO_2. Other factors that often contribute to the lower in-cylinder temperatures are the rapid burning of vaporized alcohol, combustion quenching, and charge cooling. In addition, lower exhaust temperatures at higher engine speeds are an indication of lower in-cylinder temperatures and validate an overall increase in CO emissions due to incomplete burning. Like our results, Imran et al. found reductions in CO emissions over increasing engine loads [49]. Surawski et al. found similar results where increasing FEF produced increased CO emissions, but increasing load at a constant engine speed decreased CO emissions [31].
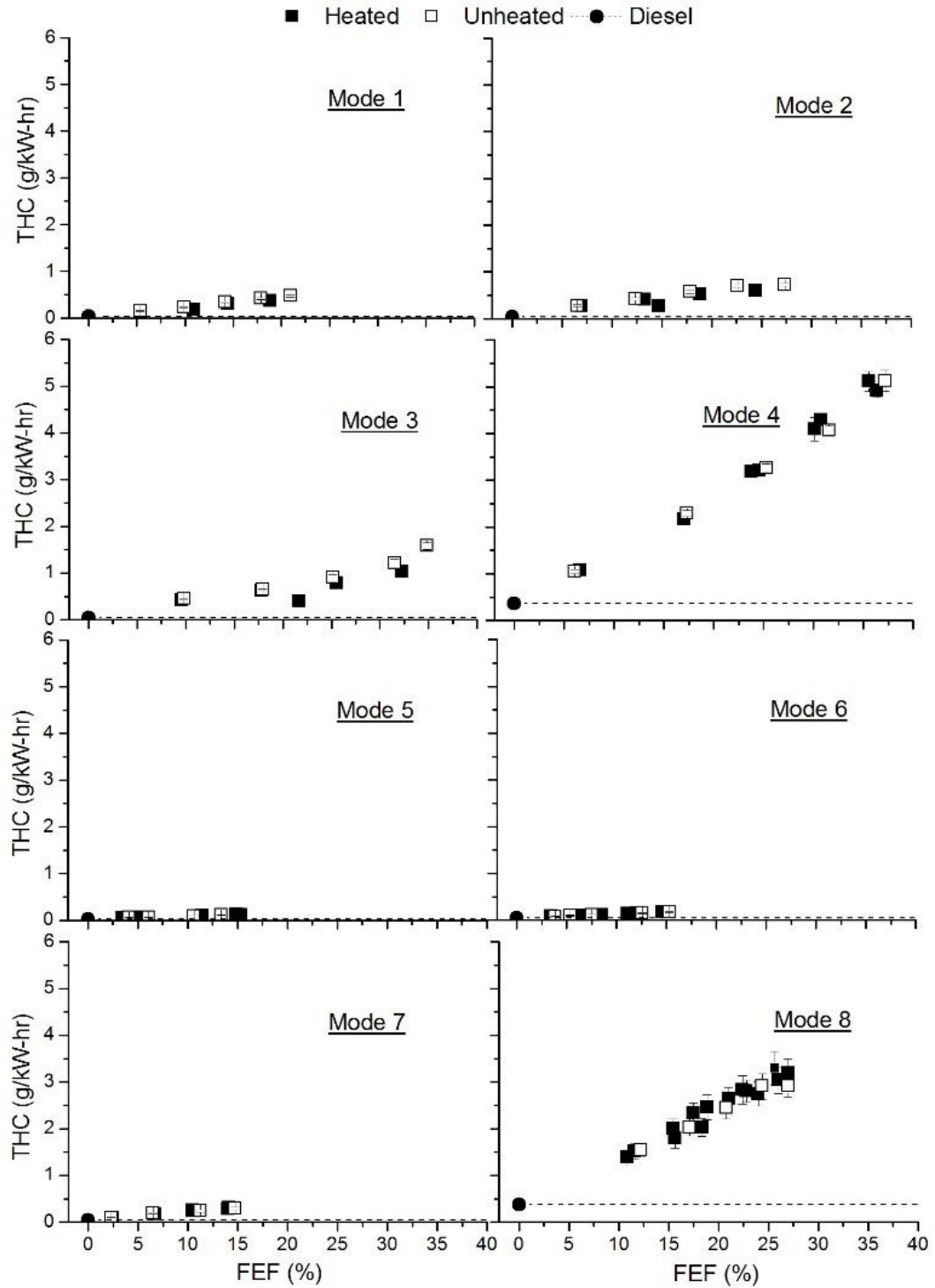
5.3.5 THC Emissions

Figure 28: Brake-specific THC emissions as measured by FT-IR in g/kW-hr for

each mode as a function of FEF

57

In previous studies, trends for HC emissions and CO emissions are usually similar, especially for intake fumigation of alcohols [49]. Figure 28 shows the THC emissions for heated and unheated ethanol injection. The THC were calculated as the sum of carbon-based species on a C1 basis, as measured by the FT-IR. Ethanol was excluded from these calculations. The results showed a clear trend of increasing THC as a function of FEF, with little to no difference between heated and unheated ethanol injection. Similar to CO emissions, Imran et al. found that quench layers of unburned alcohol may be forming in the cylinders [49]. These concentrations of unburned alcohol may be unable to ignite, resulting in incomplete combustion and the increases seen in THC. Another possible cause for the increases in THC could be the higher A/F ratios at low load conditions, where fuel and air could be mixing poorly and leaking unburned fuel directly to the exhaust.

Figure 29 details the HC distribution for unheated ethanol injection during mode 3. For internal combustion engines, greenhouse gases (GHG), in particular methane (CH_4), are a primary concern [50]. Methane draws a lot of attention because it is often an additional indication of incomplete combustion. From our results, methane emissions increased with increasing FEF. This implies that as FEF increases, a greater percentage of the total fuel may not be combusting completely, and greater amounts of unburned ethanol are reaching the exhaust.
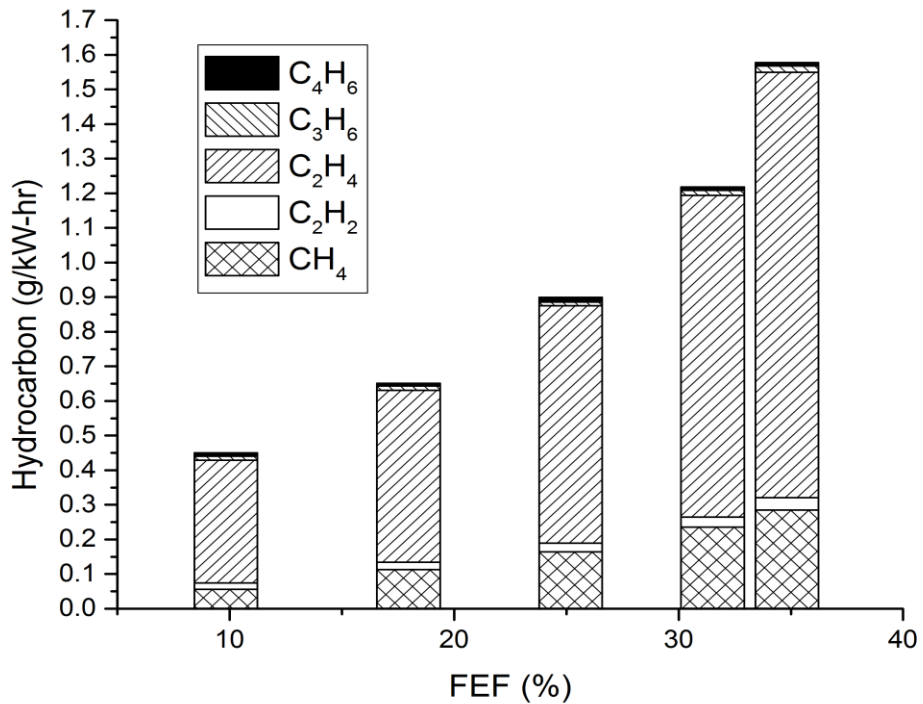
Figure 29: Individual light HC brake-specific emissions for unheated ethanol injection at Mode 3

5.3.6 Ethanol Emissions

Ethanol emissions were measured to indicate the amount of port-injected hydrous ethanol that remained unburned. Figure 30 shows the brake specific ethanol emissions across each range of FEF for each test mode. Exhaust temperatures operated directly as a function of the engine load. Ethanol emissions decreased as the exhaust temperatures increased, indicating a more complete combustion process at greater engine loads. However, ethanol emissions increased drastically with increasing FEF for low load conditions. Overall, the trends show increasing ethanol emissions as FEF and/or engine speed increases, but decreasing ethanol emissions from increasing engine loads. In

addition, these trends correspond to previous findings with ethanol fumigation [4]. One of the possible causes for the trends seen could be squish volumes, where excess ethanol remains unburned through each cycle. Squish volumes are often also seen to affect the CO and THC emissions as well. Another possible cause for incomplete combustion of the ethanol could be the ethanol's high latent heat of vaporization leading to charge cooling [49,51,52].

Kohse-Höinghaus et al. found that acetaldehyde (CH_3CHO) and formaldehyde (CH_2O) are often two products of the combustion of ethanol. Acetaldehyde is formed by H-abstraction, and formaldehyde is formed by C-C β-scission of the ethoxy radical [53]. With respect to FEF, our results found that acetaldehyde and formaldehyde were directly proportional to the ethanol emissions. Because they were directly proportional, only plots for ethanol are shown here for brevity. The maximum brake-specific concentrations for formaldehyde and acetaldehyde were during mode 4 at 36% FEF where the emissions were 11.01±0.47 g/kW-hr and 5.83±0.24 g/kW-hr, respectively.
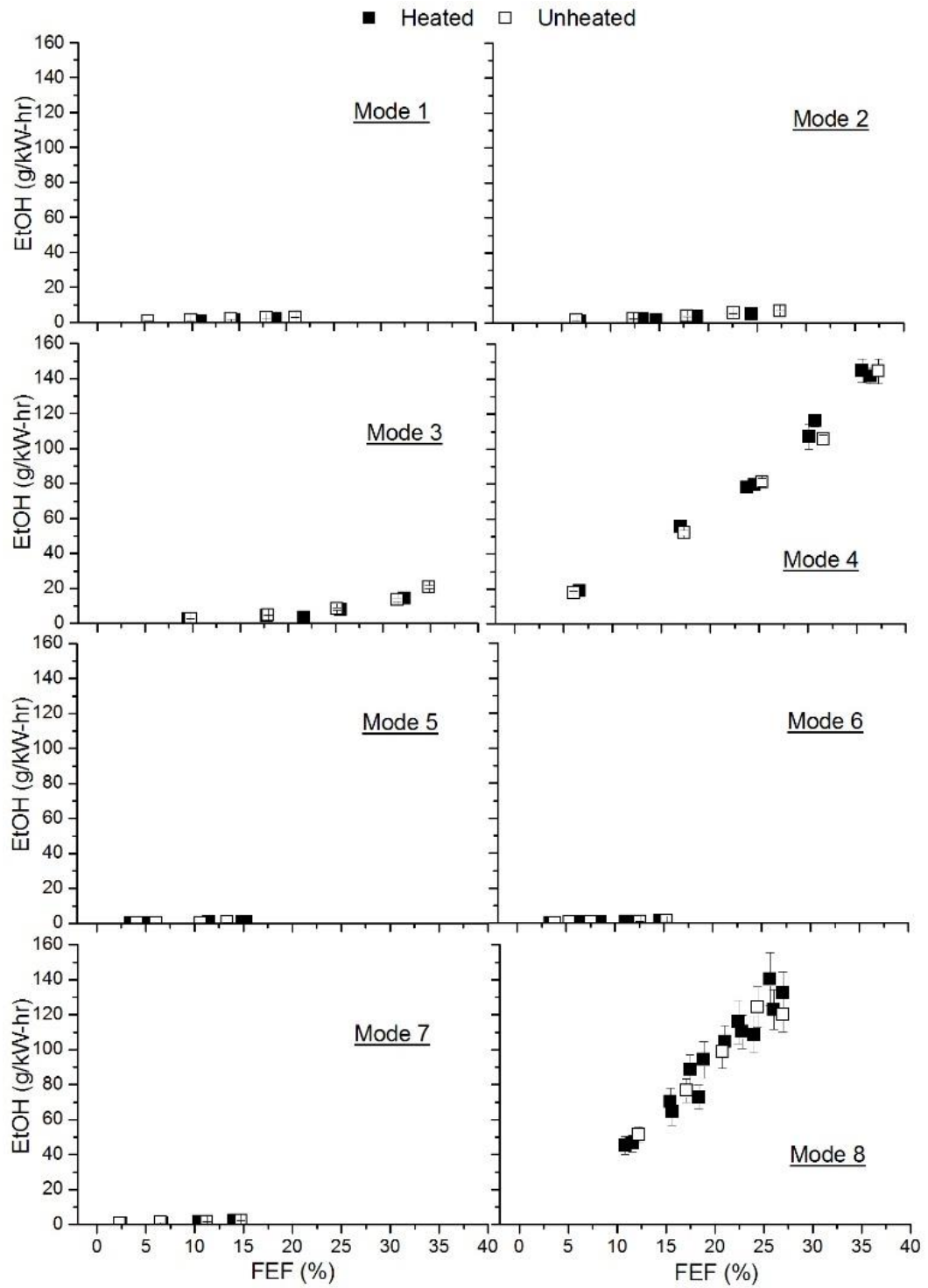
Figure 30: Brake-specific EtOH emissions as measured by FT-IR in g/kW-hr for each mode as a function of FEF

In addition, it has been found that ethanol has the potential to short circuit from intake to exhaust ports due to a positive valve overlap [54]. Increasing and decreasing valve timing and overlap would affect more than just ethanol emissions. In some cases, it has been found that HC and CO emissions are more heavily influenced by the fuel properties, as opposed to the engine output parameters, and NO_X emissions are more influenced by engine operation conditions e.g. speed, load, valve events [55]. Engine operating conditions would need to be optimized to cause beneficial results for not only ethanol emissions, but other emissions and engine performance as well.

Table 1 and Figure 31 detail the valve events for our engine and shows a 41 crank angle degree (CAD) overlap between the intake valve opening and the exhaust valve closing. Figure 31 also shows the ethanol injection minimum and maximum durations with respect to the valve timings. After determining the 0 degree position of the cam signal being read into the cRIO, the ethanol injection was adjusted to begin injection at top dead center following the exhaust stroke. Note that the x-axis of Figure 31 is in relation to top dead center firing, and that top dead center is 360 CAD after top dead center firing (ATDCF). The ethanol injections ranged from 6.0 to 345.6 CAD, depending on the engine speed. For longer pulse widths at greater engine speeds, the injection length exceeds the duration of the intake valve being open. This results in excess ethanol accumulating in the intake and entering into the next cylinder as the intake valves open. For shorter pulse widths, only half of the valve overlap has the potential to short circuit ethanol to the exhaust. For longer pulse widths, the excess ethanol from the previous cylinder's injection has the potential to short circuit to the exhaust during the entire valve overlap. This excess

ethanol short circuiting is in addition to the portion that short circuits from the dedicated cylinder's injection.
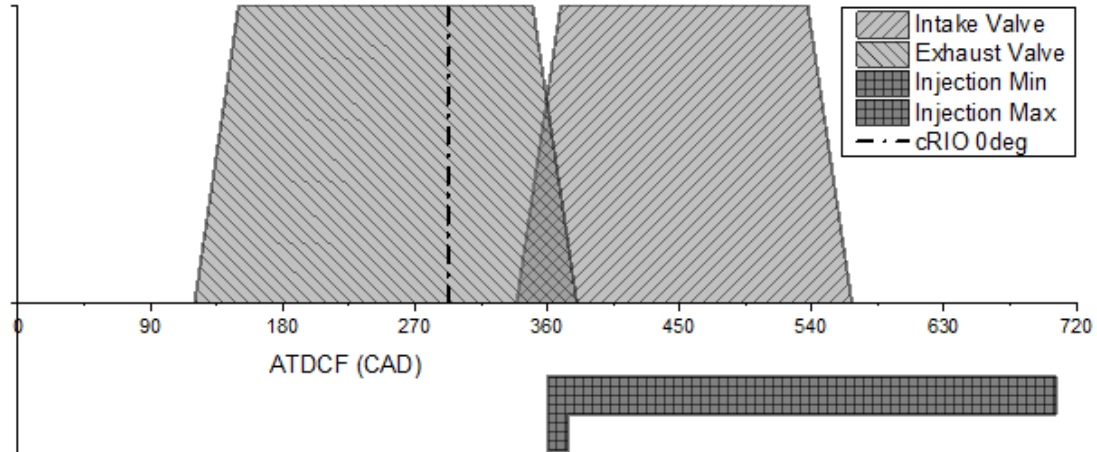
Figure 31: Intake and exhaust valve timing events and ethanol injection durations

5.3.7 Soot Emissions

Soot emissions are shown in Figure 32. For low engine speeds, soot concentrations initially increase but then decrease, with respect to FEF. For high engine speeds, soot levels had a decreasing trend with respect to FEF. El-Hagar et al. found that soot formation rates decrease with the addition of ethanol [29]. These additions of ethanol increase the charge cooling effect, and therefore, increase the ignition delay time. This increased delay allows for better mixing of diesel and ethanol, which yields better air utilization and lower soot concentrations.
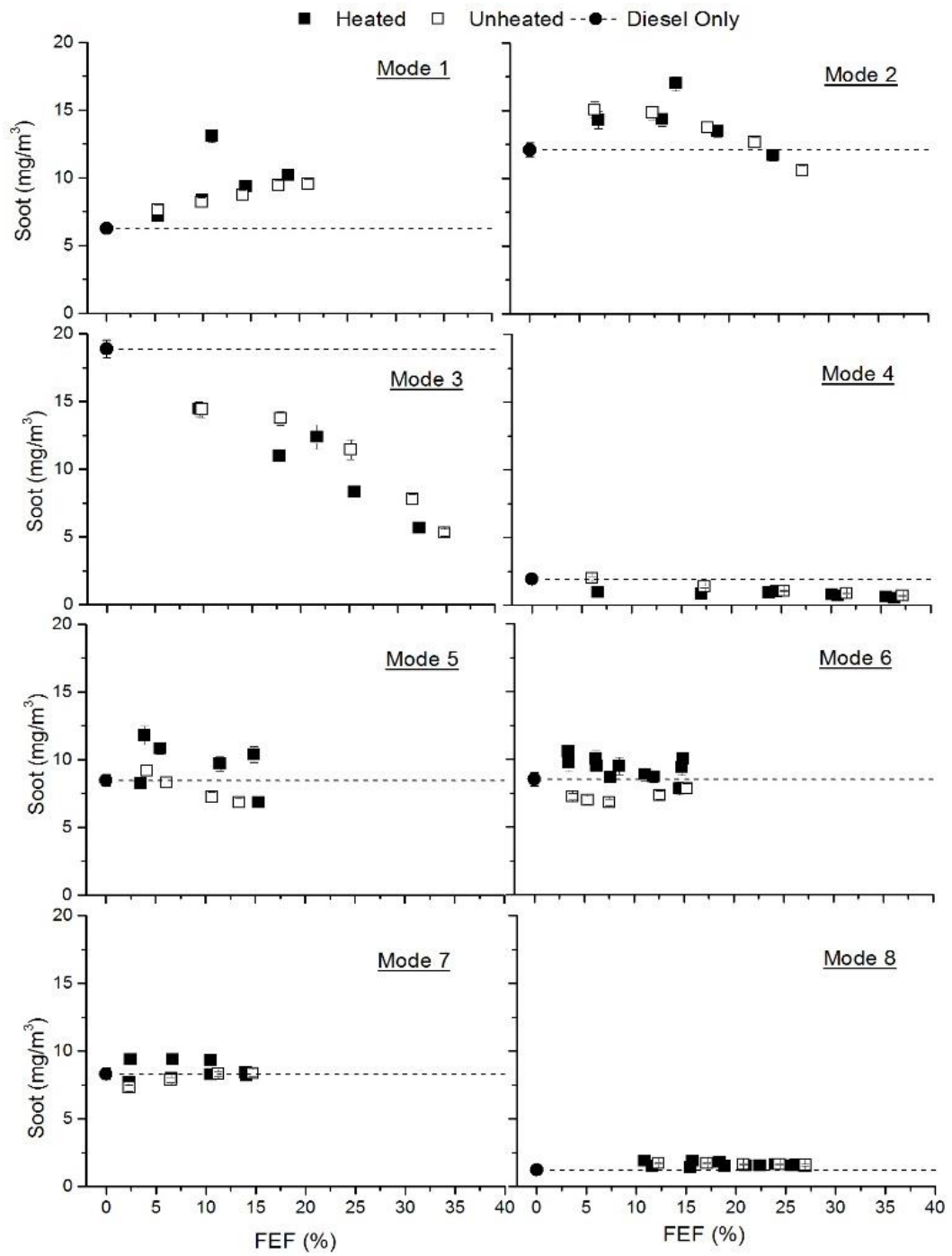
Figure 32: Soot concentration as measured by Microsoot in mg/m^3 for each mode as a function of FEF

Another common cause for these reductions in soot formation from the addition of ethanol in dual-fuel systems is often attributed to ethanol's chemical composition. Focusing on the chemical composition, Surawski et al. showed that ethanol is free of aromatics, and that the addition of ethanol results in increased OH radicals. The absence of aromatics helps suppress soot formation, and the increasing OH radicals help oxidize soot particles, which in turn reduces the concentration of soot in fuel-rich areas of the combustion chamber [31]. Ethanol (C_2H_5OH) consists of C-H, C-C, C-O, and O-H bonds. The increased amounts of OH radicals can be attributed to the C-C and C-O bonds having lower bond energies, and as a result, will more readily break during the combustion process.

Chapter 6: Conclusions

In this work, a novel heat exchanger and PFI rail combination was designed and explored for implementing dual fuel diesel engine operation with hydrous ethanol as the fumigant. Through thermal analysis, a selection of three stainless steel tubes organized in an inverted triangular fashion were found to promote the greatest amount of heat transfer and ethanol injection temperatures in the heat exchanger. The heat exchanger was found to achieve ethanol outlet temperatures in the range of 46-79°C, and performed similarly to the modeled results. Other thermal results showed that the effectiveness ranged from 0.32-0.98. Two co-flow effectiveness results achieved values less than 0.00, indicating that the ethanol outlet temperature was lower than the inlet temperature. A possible cause of this may have been cooler ambient air lowering the ethanol outlet temperature below the estimated 25°C inlet temperature. It was found that the effectiveness of the heat exchanger decreases, yet the LMTD increases with respect to the ethanol fuel flow. These opposite trends were likely caused by the design of the heat exchanger and the residence times of ethanol having a large effect.

The thermal cross-sections and velocity path lines of ethanol revealed a primarily laminar profile except for a short distance near the entrance where the flow entered a transitional Re regime. Turbulence and Reynold's Number increases may aid heat transfer, but it did not show significant effects with this heat exchanger design. Possible design changes to increase turbulence would be to implement baffles between the inlet and each outlet or using pipes with enhanced surfaces. Using baffles would create turbulence and

increase the minimum travel distance, therefore increasing the overall heat transfer. Enhanced tube surfaces would decrease the buildup of an insulating boundary layer.

With regards to engine performance, heated and unheated 180 proof hydrous ethanol was injected using said PFI rail across a modified ISO 8178 eight-point test plan and compared to the diesel only operation. It was found that FEF's of up to 37% were achievable, with only modest benefits to emissions. With respect to FEF, NO emissions decreased, whereas NO_2, CO, THC, and ethanol emissions increased. NO reductions were balanced by increases in NO_2, causing NO_X levels to remain constant. Soot showed varying trends, but with a tendency to decrease overall with increasing FEF. These trends were found for both heated and unheated ethanol injections. Preheating the ethanol using an engine coolant circulated heat exchanger showed little improvement in engine emissions. Since ethanol's latent heat of vaporization is much greater than the sensible heat, the heat exchanger did not contribute much to the overall energy required since the fuel required liquid injection. Overall, these findings indicate that aftermarket dual fuel PFI systems using hydrous ethanol and diesel fuel cannot achieve the same benefits in emission reduction as compared to low temperature RCCI combustion methods. A main reason for this is the lack of the ability to optimize the diesel fuel injection events and therefore, combustion itself.

Future research should look to increase the flow rate of the injectors, as some of the high-speed modes were limited by the capabilities of the injectors. Increasing the water content of the hydrous ethanol should also be explored to compare the effects of more water being injected. In-cylinder temperature and pressure measurements would also be

beneficial for a better indication of knock and other combustion characteristics. Finally, with fewer dimensional design constraints, a larger and better designed heat exchanger would be worth researching for the examination of the effectiveness and LMTD trends. Further the possibility of increasing ethanol temperatures beyond operating temperatures of the engine coolant to partially vaporize the ethanol may be considered. In addition, a new design and more modeling analyses would allow for a better balancing of ethanol injection temperatures between the counter-flow and co-flow injectors.

References

[1] 2016, "Weekly Retail Gasoline and Diesel Prices," U.S. Energy Inf. Adm. [Online]. Available: https://www.eia.gov/dnav/pet/PET_PRI_GND_DCUS_NUS_M.htm.

[2] Yacobucci, B. D., 2007, Fuel Ethanol : Background and Public Policy Issues Fuel Ethanol : Background and Public.

[3] 2016, "Fuel Ethanol, Corn and Gasoline Prices, by Month" [Online]. Available: http://www.ers.usda.gov/datafiles/US_Bioenergy/Prices/table14.xls. [Accessed: 04-Oct-2016].

[4] Hwang, J. T., and Northrop, W. F., 2014, "Gas and Particle Emissions From a Diesel Engine Operating in a Dual-Fuel Mode Using High Water Content Hydrous Ethanol," Volume 1: Large Bore Engines; Fuels; Advanced Combustion; Emissions Control Systems, ASME, p. V001T02A003.

[5] Saffy, H. a, Northrop, W. F., Kittelson, D. B., and Boies, A. M., 2015, "Energy , carbon dioxide and water use implications of hydrous ethanol production," Energy Convers. Manag., **105**, pp. 900–907.

[6] Curran, S., Hanson, R., Barone, T., Storey, J., and Wagner, R., 2012, Combustion Modes with Alternative Fuels: Reactivity Controlled Compression Ignition Case Study.

[7] Stone, R., 2012, Introduction to Internal Combustion Engines, Society of Automotive Engineers Inc.

[8]   McGee, J., Curtis, E., Russ, S., and Lavoie, G., 2000, "The Effects of Port Fuel Injection Timing and Targeting on Fuel Preparation Relative to a Pre-Vaporized System," Society, (724).

[9]   Braisher, M., Stone, R., and Price, P., 2010, "Particle Number Emissions from a Range of European Vehicles," Soc. Automot. Eng., (Ci).

[10]   Mathis, U., Mohr, M., and Forss, A., 2005, "Comprehensive particle characterization of modern gasoline and diesel passenger cars at low ambient temperatures," Atmos. Environ., **39**(1), pp. 107–117.

[11]   Queiroz, C., and Tomanik, E., 1997, "Gasoline Direct Injection Engines - A Bibliographical Review."

[12]   Cole, R. L., Poola, R. B., and Sekar, R., 1998, "Exhaust Emissions of a Vehicle with a Gasoline Direct-Injection Engine," SAE Tech. Pap., (982605).

[13]   Storey, J., Barone, T., Thomas, J., and Huff, S., 2012, "Exhaust Particle Characterization for Lean and Stoichiometric DI Vehicles Operating on Ethanol-Gasoline Blends," SAE Tech. Pap., (2012-01–0437).

[14]   Kasseris, E., and Heywood, J. B., 2012, "Charge Cooling Effects on Knock Limits in SI DI Engines Using Gasoline/Ethanol Blends: Part 1-Quantifying Charge Cooling," SAE Int. J. Fuels Lubr., pp. 844–854.

[15]   Stein, R. a, Polovina, D., Roth, K., Foster, M., Lynskey, M., Whiting, T., Anderson, J. E., Shelby, M. H., Leone, T. G., and VanderGriend, S., 2012, "Effect of Heat of Vaporization, Chemical Octane, and Sensitivity on Knock Limit for

Ethanol - Gasoline Blends," SAE Int. J. Fuels Lubr., **5**(2), pp. 823–843.

[16]   Alkidas, A. C., 2007, "Combustion advancements in gasoline engines," Energy
       Convers. Manag., **48**(11), pp. 2751–2761.

[17]   Ekholm, K., Karlsson, M., Tunestål, P., Johansson, R., Johansson, B., and Strandh,
       P., 2009, "Ethanol-Diesel Fumigation in a Multi-Cylinder Engine," SAE Int. J.
       Fuels Lubr., **1**(1), pp. 26–36.

[18]   Kimura, S., Kimura, S., Aoki, O., Aoki, O., Ogawa, H., Ogawa, H., Muranaka, S.,
       Muranaka, S., Enomoto, Y., and Enomoto, Y., 1999, "New combustion concept
       for ultra-clean and high-efficiency small DI diesel engines," SAE Pap. 1999-01-
       3681, **3pp**(724), p. 01-3681.

[19]   Yang, Y., Dec, J. E., Sjöberg, M., and Ji, C., 2015, "Understanding fuel anti-knock
       performances in modern SI engines using fundamental HCCI experiments,"
       Combust. Flame, **162**(10), pp. 4008–4015.

[20]   Aroonsrisopon, T., Foster, D., Morikawa, T., and Lida, M., 2002, "Comparison of
       HCCI Operating Ranges for Combinations of Intake Temperature , Engine Speed
       and Fuel Composition," SAE Tech. Pap., (2002-01–1924).

[21]   Reitz, R. D., and Duraisamy, G., 2015, "Review of high efficiency and clean
       reactivity controlled compression ignition (RCCI) combustion in internal
       combustion engines," Prog. Energy Combust. Sci., **46**, pp. 12–71.

[22]   "Nonroad Diesel Engines" [Online]. Available:
       https://www.dieselnet.com/standards/us/nonroad.php. [Accessed: 17-Dec-2015].

[23] Johnson, T. V., 2015, "Review of Vehicular Emissions Trends," SAE Int. J. Engines, **8**(3).

[24] Wang, M., Wu, M., and Huo, H., 2007, "Life-cycle energy and greenhouse gas emission impacts of different corn ethanol plant types," Environ. Res. Lett., **2**(2), p. 24001.

[25] Fang, W., Kittelson, D. B., and Northrop, W. F., 2013, "An Experimental Investigation of Reactivity-Controlled Compression Ignition Combustion in a Single-Cylinder Diesel Engine Using Hydrous Ethanol," Proceedings of the ASME 2013 Internal Combustion Engine Division Fall Technical Conference, pp. 1–9.

[26] Dempsey, A. B., Walker, N. R., Splitter, D., Wissink, M., and Reitz, R. D., 2012, "Characterization of Reactivity Controlled Compression Ignition (RCCI) Using Premixed Hydrated Ethanol and Direct Injection Diesel in Heavy-Duty and Light-Duty Engines."

[27] Rahman, M. M., Stevanovic, S., Brown, R. J., and Ristovski, Z., 2013, "Influence of Different Alternative Fuels on Particle Emission from a Turbocharged Common-Rail Diesel Engine," Procedia Eng., **56**, pp. 381–386.

[28] Abu-Qudais, M., Haddad, O., and Qudaisat, M., 2000, "The effect of alcohol fumigation on diesel engine performance and emissions," **41**, pp. 389–399.

[29] El-hagar, M. M. E., 2014, "Exhaust emissions of a single cylinder diesel engine with addition of ethanol," **3**(1), pp. 74–81.

[30] Olson, A. L., 2010, "The Effect of Ethanol-Water Fumigation on the Performance and Emissions from a Direct-Injection Diesel Engine," (September).

[31] Surawski, N. C., Ristovski, Z. D., Brown, R. J., and Situ, R., 2012, "Gaseous and particle emissions from an ethanol fumigated compression ignition engine," Energy Convers. Manag., **54**(1), pp. 145–151.

[32] Soloiu, V., Muinos, M., and Harp, S., 2015, "Investigation of Dual Fuel PCCI (PFI of n-Butanol and DI-ULSD) Compared with DI of Binary Mixtures of the Same Fuels in an Omnivorous Diesel Engine."

[33] Mukherjee, R., 1998, "Effectively Design Shell-and-Tube Heat Exchangers," Chem. Eng. Prog., **February**, pp. 21–37.

[34] "Chemical Compatibility Results" [Online]. Available: http://www.coleparmer.com/Chemical-Resistance.

[35] 2013, "Chemical Compatibility" [Online]. Available: http://www.graco.com/content/dam/graco/ipd/literature/misc/chemical-compatibility-guide/Graco_ChemCompGuideEN-B.pdf.

[36] Coelho, E. P. D., Moles, C. W., dos Santos, M. A. C., Barwick, M., and Chiarelli, P. M., 1996, "Fuel Injection Components Developed for Brazilian Fuels."

[37] "DieselNet Emission Test Cycles" [Online]. Available: http://www.dieselnet.com/standards/cycles/iso8178.php. [Accessed: 02-Oct-2015].

[38] Figliola, R., and Beasley, D., 2000, Theory and Design for Mechanical Measurements, John Wiley and Sons, New York.

[39]   Guo, Z. Y., Liu, X. B., Tao, W. Q., and Shah, R. K., 2010, "Effectiveness–thermal resistance method for heat exchanger design and analysis," Int. J. Heat Mass Transf., **53**(13–14), pp. 2877–2884.

[40]   TEMA, 1999, "Standards of the Tubular Exchanger, 8th Edition."

[41]   Greeves, G., Khan, I. M., and Onion, G., 1977, "Effects of water introduction on diesel engine combustion and emissions," Symp. Combust., **16**(1), pp. 321–336.

[42]   Hulwan, D. B., and Joshi, S. V., 2011, "Performance, emission and combustion characteristic of a multicylinder DI diesel engine running on diesel–ethanol–biodiesel blends of high ethanol content," Appl. Energy, **88**(12), pp. 5042–5055.

[43]   Bowman, C. T., 1992, "Control of combustion-generated nitrogen oxide emissions: Technology driven by regulation," Symp. Combust., **24**(1), pp. 859–878.

[44]   Lilik, G. K., Zhang, H., Herreros, J. M., Haworth, D. C., and Boehman, A. L., 2010, "Hydrogen assisted diesel combustion," Int. J. Hydrogen Energy, **35**(9), pp. 4382–4398.

[45]   Bika, A. S., Franklin, L., Olson, A. L., Watts, W., and Kittelson, D., 2009, "Ethanol ultilization in a diesel engine."

[46]   Hori, M., Matsunaga, N., Marinov, N., William, P., and Charles, W., 1998, "An experimental and kinetic calculation of the promotion effect of hydrocarbons on the NO-NO2 conversion in a flow reactor," Symp. Combust., **27**(1), pp. 389–396.

[47]   Hwang, J. T., Nord, A. J., and Northrop, W. F., 2016, "Efficacy of Add-On

Hydrous Ethanol Dual Fuel Systems to Reduce NO x Emissions From Diesel Engines," ASME 2016 Intern. Combust. Engine Fall Tech. Conf., (X), p. V001T02A007.

[48] Kittelson, D., Watts, W., Walker, A., and Twigg, M., 2012, "On-Road Evaluation of an Integrated SCR and Continuously Regenerating Trap Exhaust System."

[49] Imran, A., Varman, M., Masjuki, H. H., and Kalam, M. A., 2013, "Review on alcohol fumigation on diesel engine: A viable alternative dual fuel technology for satisfactory engine performance and reduction of environment concerning emission," Renew. Sustain. Energy Rev., **26**, pp. 739–751.

[50] Macedo, I., 1998, "Greenhouse gas emissions and energy balances in bio-ethanol production and utilization in Brazil (1996)," Biomass and Bioenergy, **14**(1), pp. 0–4.

[51] Morsy, M. H., 2015, "Assessment of a direct injection diesel engine fumigated with ethanol/water mixtures," Energy Convers. Manag., **94**, pp. 406–414.

[52] Fang, W., Huang, B., Kittelson, D. B., and Northrop, W. F., 2014, "Dual-Fuel Diesel Engine Combustion with Hydrogen, Gasoline and Ethanol as Fumigants: Effect of Diesel Injection Timing," ASME 2012 Intern. Combust. Engine Div. Fall Tech. Conf. ICEF2012-92142, **136**(August 2014), pp. 373–381.

[53] Kohse-Höinghaus, K., Oßwald, P., Cool, T. A., Kasper, T., Hansen, N., Qi, F., Westbrook, C. K., and Westmoreland, P. R., 2010, "Biofuel Combustion Chemistry: From Ethanol to Biodiesel," Angew. Chemie Int. Ed., **49**(21), pp.

3572–3597.

[54]   Siewert, R., 1971, "How Individual Valve Timing Events Affect Exhaust Emissions," SAE Tech. Pap. 71060.

[55]   Deng, B., Yang, J., Zhang, D., Feng, R., Fu, J., Liu, J., Li, K., and Liu, X., 2013, "The challenges and strategies of butanol application in conventional engines: The sensitivity study of ignition and valve timing," Appl. Energy, **108**, pp. 248–260.